SPATIAL AND TEMPORAL VARIABILITY OF EXTREME WEATHER IN THE UNITED STATES

BY

Cassandra Jo Wilson

Submitted to the graduate degree program in Geography and the Graduate Faculty of the University of Kansas in partial fulfillment of the requirements for the degree of Master of Science in Atmospheric Science

---

Dr. Nathaniel A. Brunsell
Chairperson

Dr. David B. Mechem

Dr. C. Bryan Young

Date Defended: July 12, 2013

The Thesis Committee for Cassandra Jo Wilson
certifies that this is the approved version of the following thesis:

SPATIAL AND TEMPORAL VARIABILITY OF

EXTREME WEATHER IN THE UNITED STATES

Dr. Nathaniel A. Brunsell
Chairperson

Dr. David B. Mechem

Dr. C. Bryan Young

Date Approved: July 12, 2013

ABSTRACT

The United States Historical Climate Network (USHCN) station data from 1900-2011 is used to quantify trends in daily extreme heat events, daily extreme cold events, and extreme daily precipitation within the contiguous United States. Climate data was spatially aggregated into respective Koeppen-Geiger climate zones where the 3 main zones are; arid, warm temperate and snow. Results show a gain or loss of 20 extreme temperature events and a gain or loss of 4 extreme precipitation events. Paired t-test results indicate statistically significant shifts in the magnitude of extreme weather events in each of the 3 main climate zones (arid, warm temperate and snow). Teleconnection patterns that directly impact US weather are El Niño Southern Oscillation (ENSO) and Pacific Decadal Oscillation (PDO). The use of wavelet analysis, including the continuous wavelet transform, the wavelet cross wavelet transform and the wavelet transform coherence provide insight into the timescales of influence from ENSO and PDO on extreme weather events. Results indicate that extreme precipitation events have significantly different power spectras than normal events across all timescales. Specific patterns at the annual scale and shorter are found the arid zone for extreme maximum temperature, where results for minimum temperature trends vary.

ACKNOWLEDGMENTS

This research was possible thanks to funding provided by the US Department of Energy (DOE), grant DE-SC0005359. As well as additional support from the National Science Foundation (NSF) Experimental Program to Simulate Competitive Research (EPSCoR) grants, NSF EPS-0553722, EPS-09194443, KAN0061396 and KAN0066263. I would like to express my deepest gratitude to my advisor Dr. Nathaniel A. Brunsell for the abundant encouragement, support and guidance. I would also like to thank the members of my committee, Dr. David B. Mechem and Dr. C. Bryan Young for their added knowledge, assistance and patience. Special thanks to Dr. Lee M. Miller for his many wise words throughout this process. Last but not least, I would like to thank my family and Steven for their unwavering support and encouragement, none of this would have been possible without it.

Contents

List of Figures

List of Tables

Chapter 1

Introduction

The Earth's climate is a complex system and is faced with future change. Extreme weather patterns is one area of this system that is not well understood. The Intergovernmental Panel on Climate Change (IPCC) has concluded, "the frequency of heavy precipitation events has increased over most land areas, consistent with warming and observed increases of atmospheric water vapor. Widespread changes in extreme temperatures have been observed over the last 50 years. Cold days, cold nights and frost have become less frequent, while hot days, hot nights and heat waves have become more frequent" (IPCC, 2007). The issue then resides in the ability to scale this global information down to regional and local impacts.

Due to the large geographic area and variation in climate within the United States (US), extreme weather is expected to vary spatially. As witnessed on the West Coast of North America, climate change has affected regions differently, a trend towards more or less extreme precipitation with warmer or cooler temperature extremes (Booth et al., 2011). Portmann et al. (2009) have provided strong evidence that extreme trends within the United States are linked to the hydrologic cycle as well as seasonal and latitudinal classifications. Allan and Soden (2008) found that

changes in extreme precipitation events in response to global climate change may in fact be under-predicted. Not only do the changes in the frequency of extreme events need to be quantified but also the change in the magnitude of the events. In order to understand the regional dependence of climate extremes within the US, this thesis focuses on the trends in extreme statistics (magnitude threshold and frequency of occurrence), as well as an analysis of those characteristics by climate zone (Koeppen-Geiger classification). Understanding past changes in these statistics will provide insight into which climatic regions are the most susceptible to extreme weather in a warming world.

Blekinsop et al. (2008) have shown that forcing mechanisms such as regional circulation patterns impact the climate, and may also impact the distribution of extreme weather events. Regional circulations are often impacted by teleconnection patterns such as El Niño/Southern Oscillation (ENSO), Pacific Decadal Oscillation (PDO), North Atlantic Oscillation (NAO), and the Atlantic Multidecadal Oscillation (AMO). Since midlatitude climate extremes have been shown to be associated with these low-frequency teleconnection patterns, it is important to study these patterns as possible forcing mechanisms and the temporal variation they may cause on extreme weather events. One teleconnection in particular, PDO, has been shown to influence the precipitation patterns of the West Coast of America (Mantua et al., 1997) as well as the Desert Southwest (Meehl et al., 2010). Specifically, summer precipitation extremes in the western US are most influenced by PDO (Nigam et al., 1999). Higher frequency teleconnection patterns, such as ENSO, tend to have similar influences on the regional circulation patterns. During strong ENSO signals, the United States is impacted by either drier and warmer conditions or cooler and wetter conditions. These climate impacts depend on the ENSO signal, negative signifying an El Niño signal (warm and dry) and positive signifying a La Niña signal (cool and wet). PDO

follows similar patterns and can either intensify or weaken the ENSO signal. Not only do strong phases interact with regional circulation patterns to produce extreme events, but the change between these phases can also impact the weather and, potentially, extreme weather. To understand the covariability of teleconnections and extreme weather, a technique that can isolate influences across different time scales is required. One method is the use of wavelet decomposition. Wavelet analysis allows the variation between the geographical patterns of extreme events and low frequency teleconnection patterns to be quantified.

In order to better understand extreme weather events, this thesis will address the following questions: 1. Is there a change in the frequency of extreme weather events from 1900-2011, and how do the distributions vary as a function of climate zone? and 2. What is the temporal and spatial variability imposed by teleconnection patterns on extreme weather?

Chapter 2

Trends in 20th Century Weather Extremes over the Continental United States

2.1 Introduction

Natural and anthropogenic forcings have impacted the climate and have the ability to cause significant changes to extreme weather events within the United States (US) (IPCC, 2001). The rate of warming for the 21st century is projected to be several times greater than the 20th century, and the impact this warming will have on extreme weather needs to be quantified. The Intergovernmental Panel on Climate Change (IPCC) has concluded, "the frequency of heavy precipitation events has increased over most land areas, consistent with warming and observed increases of atmospheric water vapour. Widespread changes in extreme temperatures have been observed over the last 50 years. Cold days, cold nights and frost have become less frequent, while hot days, hot nights and heat waves have become more frequent" (IPCC, 2007).

Anthropogenic climate change can alter the hydrologic cycle which creates complications for future extreme events (Allan and Soden, 2008). The Clausius-Clapeyron relationship can help to explain the governing components for the upper limits within the atmospheric portion of the hydrologic cycle. The Clausius-Clapeyron relationship provides insight into the delicate balance between atmospheric water vapor content and temperature. Since water vapor is a greenhouse gas, as temperature rises so does the potential for atmospheric water vapor content, creating an important feedback within the hydrologic cycle (Held, 2000). Atmospheric moisture has increased by 0.41 kg/m^2 per decade since 1988 and a magnitude of this nature cannot be explained by natural climate variability alone (Santer et al., 2007). In a warming world, precipitation distributions are projected to shift toward more intense events (Chou et al., 2012). The projected range of global warming based on all 6 of the IPCC Fourth Assessment Report Special Report on Emission Scenarios (AR4 SRES) is $1.4 - 5.8\,^{\circ}C$ (Knutti et al., 2008). In the Netherlands, changes in the hydrologic cycle have shown that one-hour precipitation extremes exceed the Clausius-Clapeyron relationship (Lenderink and van Meijgaard, 2008). There is strong evidence that extreme trends within the US are linked to the observed evolution of the hydrologic cycle as well as seasonal and latitudinal classifications. This evidence points to large difference in trends in minimum and maximum temperatures which can be strongly dependent on different latitudinal classifications (Portmann et al., 2009).

The increase of greenhouse gases in the past century due to anthropogenic activity has caused the temperature of the Earth to increase. The influence of anthropogenic forcing is detectable in the influence on extreme temperatures (Zwiers et al., 2011). When comparing past temperature trends from, 1901-1950 and 1971-2003, there has been a significant warming of global temperature indices (Alexander et al., 2006). The projected rate of warming under current emission scenarios is $2\,^{\circ}C$, and extreme events

for North America are projected to increase $2-6\,^{\circ}\mathrm{C}$ by the end of the century (Clark et al., 2010). As the distribution of temperatures shifts, it is estimated that current seasonal extremes will become the norm for 70-80% of the land surface (Anderson, 2011).

Extreme weather events such as extreme daily precipitation, extreme heat days, and extreme cold days may change by different magnitudes. The 21st century Community Climate System Model version 3 (CCSM3) results predict a ratio of record highs to lows to be 20:1 by mid-century and 50:1 by the end of the century (Meehl et al., 2009). Karl et al. (1995) found an increase of 9 percent for daily precipitation totals, which was later shown to be a product of an increase in extreme precipitation within the Continental US (Knight, 1998). Other studies have agreed on a general increase in extreme precipitation (Groisman et al., 2001, 2012; Kunkel et al., 1999, 2003).

Future climate is likely to include local changes to the intensity, frequency and amount of extremes (Trenberth and Dai, 2003). Change to extreme events can arise from anthropogenic effects or natural variability. Recent change in observed temperature extremes, specifically a decrease in frost days and an increase in warm nights/heat days, can be linked to an increase in greenhouse gases (Meehl et al., 2007a). Natural events also impact extreme weather. Global models have been used to simulate 21st century climate which induces low-frequency variability like El Niño Southern Oscillation (ENSO) events. These simulations show stronger precipitation prevalent in the southern states, accompanied by an increase in heat waves in correspondence with El Niño events (Meehl et al., 2007b).

Future increases in extreme events are predicted, but changes in extreme precipitation events, in response to global warming may be in fact under-predicted by models (Allan and Soden, 2008). Tebaldi et al. (2006) observed a link between green house

gas emissions and magnitudes in extreme temperatures across 9 Global Climate Models (GCMs). They also noted projected temperature extremes within North America, specifically in the southwest. The 9 GCMs also projected a world characterized by intensified precipitation, with significant increases in the high latitudes of the Northern Hemisphere.

On a global scale, it is accepted that an increase in extreme precipitation events will be seen (Groisman et al., 2001, 2012; Kunkel et al., 1999, 2003), but the regional behavior of temperature and precipitation extremes is not well understood. Climate can create regional differences when and where certain extremes occur based on the precipitation and temperature regimes present. For example, the greatest excess of record highs are pronounced in the midwest during February, while excess record lows exist in the southeast during October (Anderson and Kostinski, 2011). One study found that in the Northeastern US, extreme precipitation is projected to increase in winter and exhibit no change or decrease in the summer, alongside 20-40 more extreme heat events each year by the end of the 21st century (Hayhoe et al., 2006). As witnessed on the North American west coast, climate change has affected regions differently, resulting in a trend towards more or less extreme precipitation with warmer or cooler temperature extremes (Booth et al., 2011).

In order to understand the regional dependence of climate extremes within the US, this study focuses on the trends in extreme statistics (magnitude threshold and frequency of occurrence), as well as an analysis of those characteristics by climate zone (Koeppen-Geiger classification). Understanding past change in these statistics will provide insight into which climatic regions are the most susceptible to extreme weather in a warming world. This thesis is a detailed study of changes in extreme weather for the US using data from the United States Historical Climate Network (USHCN) and assess these variations as a function of geographic and climatic region.

2.2 Data

Research was conducted for extreme weather events within the US using the USHCN network. Data for the USHCN was assembled from existing stations by the National Oceanic and Atmospheric Administration (NOAA) National Climatic Data Center (NCDC) in order to better detect climate change (Menne et al., 2011). The USHCN consists of 1,218 towers across the continuous US, which collect daily measurements of maximum temperature, minimum temperature, precipitation amount, snowfall amount, and snow accumulation. For this study only maximum temperature, minimum temperature and daily precipitation were examined. Stations missing more than 10 years were eliminated. This analysis left 958 USHCN stations for long-term analysis of the variability of extreme events.

Quantifying extreme events as a function of regional climate requires aggregating the stations according by climate classification. The most common way to classify climate is the Koeppen-Geiger (KG) classification system (Kottek et al., 2006). The KG system helps explain the different regional climate impacts that extreme weather has within the US. The US consists of 14 different KG zones, but 95% of the country lies in just 9 climate zones. For this research, the station data was aggregated into nine KG zones. The distribution of USHCN station coverage and applicable KG zone can be found in Figure 2.1. The main classification regions are: B-arid, C-warm temperature and D-snow. The precipitation classification groups are: W-desert, S-steppe, f-fairly humid and s-summer dry. The temperature classification groups are: h-hot arid, k-cold arid, a-hot summer and b-warm summer. The selected climates represent 95% of the area within the US are: BSh, BSk, BWh, BWk, Cfa, Csa, Csb, Dfa and Dfb.

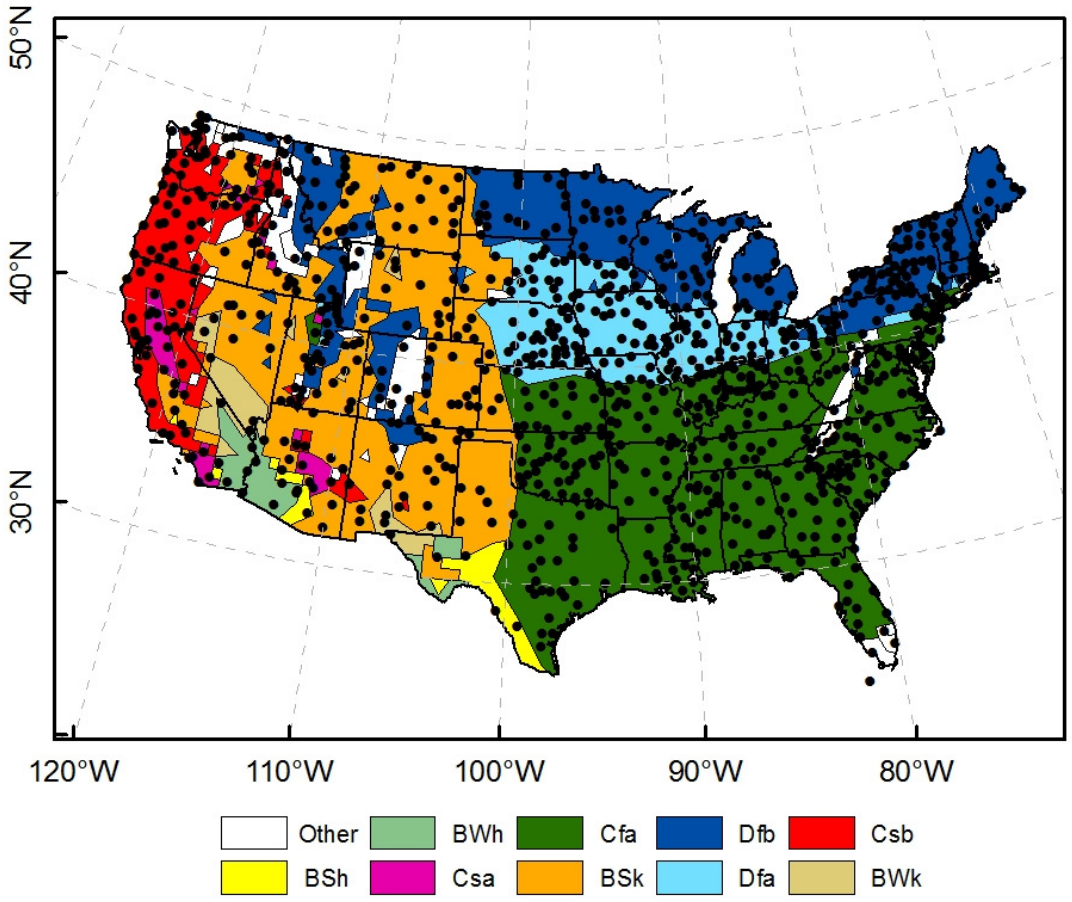

Figure 2.1 USHCN station distribution with corresponding Koeppen-Geiger classification.

2.3 Methodology

2.3.1 Overview

A statistical analysis of daily precipitation, maximum temperature and minimum temperature within the US was conducted to evaluate the past nature of extreme events. The changes in the extreme events were examined from 1900-2011 by analyzing the 90th percentile of precipitation and maximum temperature, and the 10th percentile for minimum temperature. A quantile analysis of the data set was used to calculate the extreme events per month per station. A linear regression was then used to analyze the change in the number of events that exceeded the respective extreme threshold. A Mann-Kendall test was used to assess the significance of the linear trends. In order to assess for stationarity the data were divided into two time periods, 1950-1980 and 1980-2011. Using a paired t-test, the probability density function (PDF) of each time period was analyzed. The stationarity examination looks at how the magnitude thresholds have changed over time, in order to quantify the relative influence of climate change.

2.3.2 Extreme Analysis

The IPCC bases its definition of extreme events on the frequency of occurrence of the event (IPCC, 2007). Using this definition, frequency of occurrence above the 90th percentile (precipitation and maximum temperature) or below the 10th percentile (minimum temperature) was examined. Extreme events were calculated by establishing monthly threshold values for each station. For example, each station will have a threshold value corresponding to a 90th percentile of maximum temperature per season. This allows for an analysis that accurately follows a seasonal cycle of yearly changing magnitude thresholds specific to each station and climate. For sea-

sonal classification; Winter is defined by DJF, spring MAM, summer JJA and fall SON. It is important to do this analysis by station in order to assess specific climate and seasonal trends because an extreme event in the winter will not have the same distribution as an extreme event in the summer.

In order to assess how the number of extreme events in the last century behaved, a linear regression of the number of events exceeding the magnitude threshold was performed. The slope from this linear regression shows the change in the number of events above the extreme magnitude threshold for the past years of record. This method of determining extreme event behavior was calculated for precipitation, maximum temperature and minimum temperature.

For precipitation it is important to note that long persistent rain, dry spells and individual events can all be considered "extreme", but in this study addresses only daily heavy rain events. Daily extreme rainfall events are important to study because they have been correlated with damaging floods (Pielke and Downton, 2000). Maximum and minimum temperature extremes were analyzed on only the daily time scale, meaning the statistics did not fully capture the behavior of extreme heat or cold days over multi-day or multi-week periods.

2.3.3 Statistical Analysis

In order to filter results at the 95% significance level was performed Mann-Kendall and paired t-tests. The Mann-Kendall evaluated the significance of the trend in number of events that exceed the magnitude threshold. The Mann-Kendall test is used because it has been found to be less affected by outliers due to the fact it is based on the sign of differences, and not based on the values themselves (Onoz and Bayazit, 2003). This test was performed using the Kendall package within the R-Project for Statistical Computing. The resulting slope values used in the trend analysis are all

significant at the p-value ≤ 0.05.

Two time periods were used in order to assess for stationarity of extreme magnitudes, 1950-1980 and 1980-2011. A paired t-test was used to assess the significance of differences between the time periods. The change in magnitude threshold level was compared between the two time periods. The difference in threshold is considered significant when the p-value ≤ 0.05, meaning the data set was non-stationary which denotes a shift in the extremes.

2.4 Results

2.4.1 Overview

The results will be discussed by grouping the climate zones based on the primary KG classification (arid zone, warm temperate zone and snow zone). The arid zone consists of 157 stations across 4 KG regions. These regions are BSh (6 stations), BSk (135 stations), BWh (6 stations) and BWk (10 stations) and are located in the desert southwest as well as a majority of the Rocky Mountains, excluding the high altitudes. The warm temperate zone consists of 433 stations across 3 KG regions. These regions are Cfa (337 stations), Csa (13 stations) and Csb (83 stations) and are located across the pacific coast as well as within the southeastern US. The final zone is snow which contains 331 stations, Dfa (148 stations) and Dfb (183), which are located in the most northern as well as the highest altitudes of the US (Figure 2.1).

The seasonality of the magnitude threshold and the slope values are shown for significant trends in Figures 3.2-3.7. The magnitude values are the thresholds needed for the weather event to be considered extreme. The definition of slope is the change in number of extremes per record length [number of extremes/year]. The magnitude and slope analyses were done for significant trends based off a Mann-Kendall p-

value ≤ 0.05. Extreme precipitation is discussed in section 2.4.2, extreme maximum temperature in section 2.4.3 and extreme minimum temperature in section 2.4.4.

Each KG region is impacted by extreme weather events differently and the strength of the impact changes on a seasonal basis. A further examination of each climate zone can be found in section 2.4.5. This section utilizes the trends in all 921 stations, significant and non-significant, and allows for a more in-depth regional analysis (Figures 3.8-3.10).

The influence of climate change is assessed by the stationarity analysis and is discussed in 2.4.6. An analysis of two recent time periods, 1950-1980 and 1980-2011, highlights which KG region(s) show significant changes (Figure 11). The paired t-test results with an asterisk (*) are indicative of 95% confidence that non-stationarity exists, that is, a difference exists between the two sampled groups.

2.4.2 Extreme Precipitation

Seasonal Variation in Magnitude

The significant magnitude thresholds for seasonal extreme daily precipitation range from $\leq$10 mm to $\geq$40 mm within the US (Figure 2.2). The warm temperate climates show the highest threshold levels year-round. The lowest threshold levels are found in the arid and snow zones, with the snow zones being slightly greater. The lowest threshold values occur during the winter and fall seasons while a majority of the high thresholds occurs during the summer. The average threshold value, stratified by season, is shown in Table 2.1 for each Koeppen-Geiger region. In the winter the lowest average threshold value is 7.61 mm occurring in the arid zone, while the highest is 24.96 mm within the warm temperate zone. For the spring the average threshold ranges from 12.76 mm to 27.27 mm and are both found in the warm temperature zone.

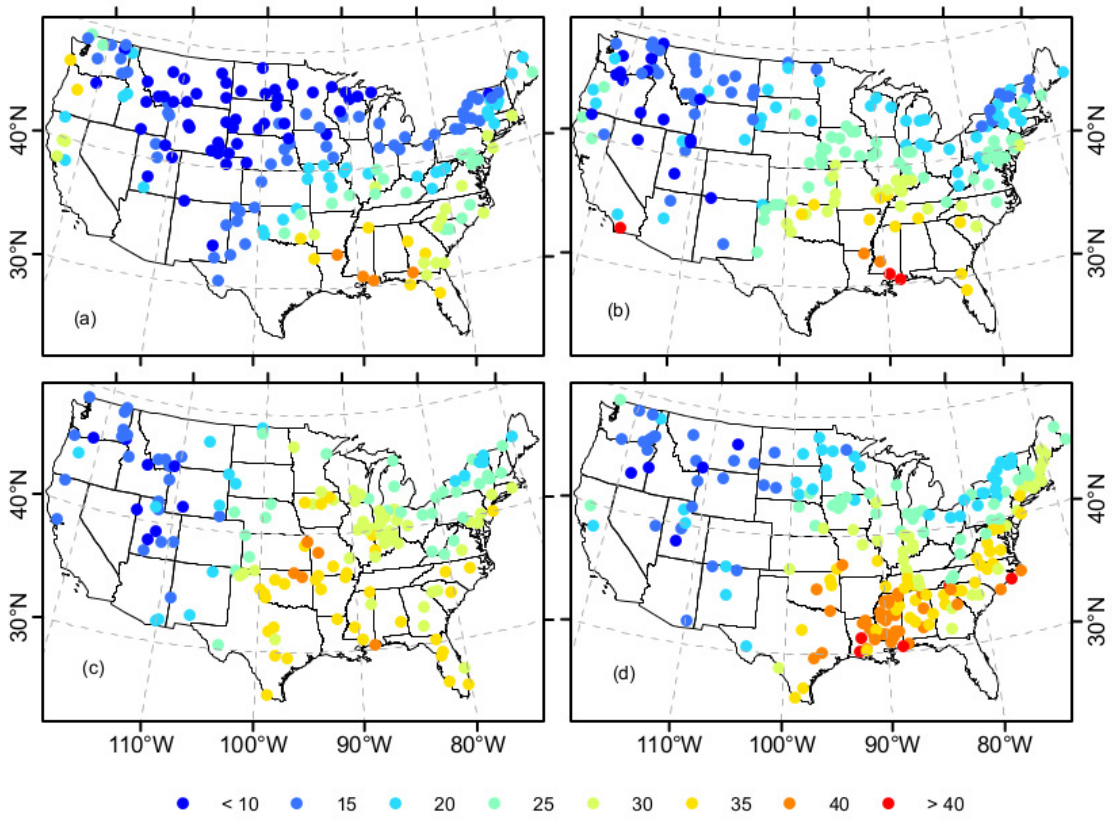

Figure 2.2 Magnitude threshold for an extreme precipitation event to occur [mm]. (a) Winter (178 significant stations), (b) Spring (171 significant stations), (c) Summer (156 significant stations) and (d) Fall (202 significant stations). Significant stations indicated by a Mann-Kendall p-value ≤ 0.05.

Month	**BSh**	**BSk**	**BWh**	**BWk**	**Cfa**	**Csa**	**Csb**	**Dfa**	**Dfb**
January	NA	7.54 (18)	NA	10.41 (1)	25.25 (40)	20.29 (1)	18.80 (4)	10.76 (11)	10.15 (24)
February	NA	7.68 (26)	NA	10.67 (1)	23.19 (32)	21.93 (2)	18.84 (7)	12.99 (20)	10.38 (26)
March	NA	11.49 (18)	NA	10.41 (1)	25.91 (40)	NA	15.43 (6)	16.16 (22)	14.02 (28)
April	NA	11.55 (17)	NA	14.86 (2)	27.12 (26)	20.83 (2)	12.53 (8)	20.40 (31)	15.61 (26)
May	23.37 (1)	14.03 (10)	NA	NA	27.47 (53)	11.09 (2)	12.16 (10)	21.71 (18)	15.30 (19)
June	NA	15.61 (11)	NA	NA	31.23 (36)	34.80 (1)	13.22 (7)	26.81 (12)	18.78 (22)
July	NA	18.06 (14)	7.87 (1)	7.57 (1)	29.48 (33)	NA	10.98 (5)	28.02 (21)	18.37 (15)
August	NA	18.16 (16)	NA	16.26 (1)	31.29 (33)	NA	11.54 (7)	25.96 (9)	20.12 (23)
September	39.62 (1)	14.22 (6)	NA	14.99 (1)	31.91 (56)	12.45 (1)	16.00 (7)	25.98 (16)	18.98 (19)
October	27.74 (1)	14.61 (8)	NA	10.16 (1)	34.95 (31)	14.36 (3)	15.15 (7)	20.56 (12)	19.17 (35)
November	17.07 (1)	8.63 (6)	NA	8.74 (1)	30.25 (60)	NA	11.46 (2)	16.93 (16)	15.51 (40)
December	NA	7.91 (13)	NA	13.97 (1)	24.56 (30)	24.38 (2)	22.34 (8)	12.74 (15)	11.06 (32)
Season	**BSh**	**BSk**	**BWh**	**BWk**	**Cfa**	**Csa**	**Csb**	**Dfa**	**Dfb**
Winter	NA	7.61 (34)	NA	11.18 (1)	24.96 (51)	24.83 (3)	18.69 (11)	12.36 (26)	11.10 (52)
Spring	NA	13.53 (26)	NA	NA	27.27 (55)	23.72 (5)	12.76 (15)	20.64 (29)	15.18 (41)
Summer	31.37 (1)	16.80 (20)	NA	16.76 (1)	30.57 (59)	34.29 (1)	11.84 (11)	26.95 (28)	19.19 (35)
Fall	30.05 (2)	12.73 (10)	NA	10.16 (1)	33.19 (99)	15.05 (4)	11.63 (5)	22.09 (27)	18.70 (54)

Table 2.1 Mean magnitude threshold for an extreme precipitation [mm] event to occur within each Koeppen-Geiger region. The parenthesis indicate the number of significant stations and NA values indicate no significant stations for reference. All values shown are significant at the 95th percentile.

The average summer thresholds vary across the warm temperate zone and range from 11.84 mm to 34.29 mm. In the fall the arid zone has the average lowest threshold at 10.16 mm while the warm temperate zone has the average highest threshold at 33.19 mm (Table 2.1).

The **arid zone** average threshold shows that the lowest thresholds are in the fall and highest in the summer. Seasonal extreme precipitation thresholds for BSh region (winter and spring), BWh region and BWk region (spring) are largely unrepresented, because lack of statistical significance. The arid climate shows little variation in seasonal thresholds for significant stations within BSh, BSk and BWk regions. The lowest average threshold for an extreme precipitation event for this zone is 7.61 mm and occurs in the BSk region (34 significant stations) during the winter, while the highest occurs in the BSh region (1 significant station) during the summer and is 31.37 mm.

The **warm temperate zone** receives the highest annual rainfall rates and thus requires the largest threshold for an extreme precipitation event to occur. The threshold in the warm temperate zone varies by season as much as 10 mm. The lowest thresholds are found in the fall and the highest during the summer. The lowest average threshold for an extreme precipitation event can be found in the Csb region (5 significant stations) during the fall (11.63 mm). The highest threshold (34.29 mm) occurs during the summer season over the Csa region (1 significant station).

Thresholds over the **snow zone** are smaller but also range by approximately 10 mm across season also. The seasonality present in this zone produces lower threshold levels within the cooler months and higher threshold levels for the warmer months. The lowest average threshold for an extreme precipitation event is found during the winter across the Dfb region (11.10 mm) (52 significant stations). The largest average threshold occurs during the summer over the Dfa region (26.95 mm) (28 significant

stations).

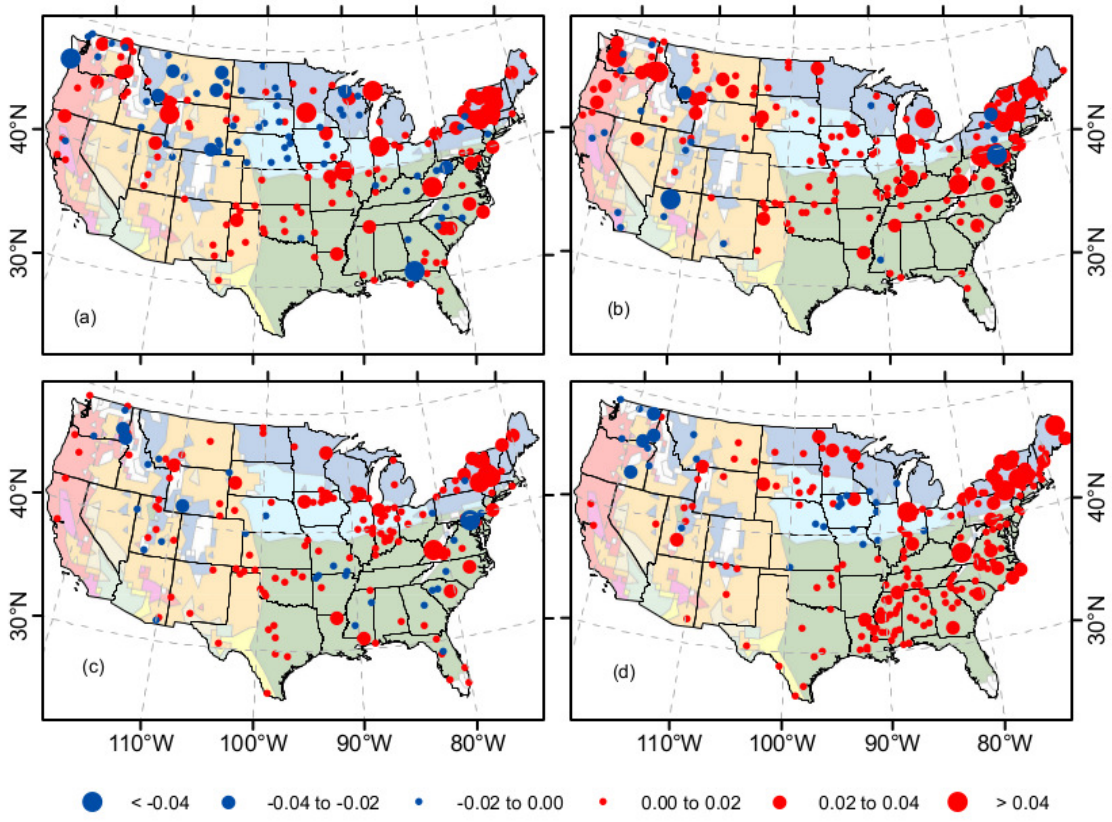

Figure 2.3 Slope of extreme precipitation events [number of extremes/year]. (a) Winter (178 significant stations), (b) Spring (171 significant stations), (c) Summer (156 significant stations) and (d) Fall (202 significant stations). Significant stations indicated by a Mann-Kendall p-value ≤ 0.05. Koeppen-Geiger classification are shown faded in bottom layer.

Seasonal Variation in Slope

The change in frequency of extreme precipitation events is shown in Figure 2.3. The slope values range from $\leq$-0.04 to $\geq$0.04 [number of extremes/year], showing a decrease/increase of 4 extreme precipitation events per century, where the average station length is 100 years. The warm temperate zone and snow zone contain the most significant stations impacted by a change in extreme precipitation. Table 2.2 shows

Month	**BSh**	**BSk**	**BWh**	**BWk**	**Cfa**	**Csa**	**Csb**	**Dfa**	**Dfb**
January	NA	$4.32 \cdot 10^{-04}$	NA	$3.47 \cdot 10^{-03}$	$6.96 \cdot 10^{-03}$	$4.06 \cdot 10^{-03}$	$9.36 \cdot 10^{-03}$	$1.39 \cdot 10^{-03}$	$5.92 \cdot 10^{-03}$
February	NA	$-1.86 \cdot 10^{-03}$	NA	$2.49 \cdot 10^{-03}$	$4.17 \cdot 10^{-03}$	$5.70 \cdot 10^{-03}$	$-1.86 \cdot 10^{-02}$	$3.10 \cdot 10^{-03}$	$2.50 \cdot 10^{-03}$
March	NA	$4.99 \cdot 10^{-04}$	NA	$-4.46 \cdot 10^{-03}$	$7.28 \cdot 10^{-03}$	NA	$1.71 \cdot 10^{-02}$	$4.85 \cdot 10^{-03}$	$1.11 \cdot 10^{-02}$
April	NA	$3.61 \cdot 10^{-03}$	NA	$-2.74 \cdot 10^{-03}$	$4.16 \cdot 10^{-03}$	$-2.64 \cdot 10^{-04}$	$1.26 \cdot 10^{-02}$	$9.52 \cdot 10^{-03}$	$8.69 \cdot 10^{-03}$
May	$-7.22 \cdot 10^{-03}$	$4.37 \cdot 10^{-03}$	NA	NA	$6.92 \cdot 10^{-03}$	$5.15 \cdot 10^{-03}$	$1.03 \cdot 10^{-02}$	$8.37 \cdot 10^{-03}$	$4.53 \cdot 10^{-03}$
June	NA	$4.01 \cdot 10^{-04}$	NA	NA	$5.54 \cdot 10^{-03}$	$8.02 \cdot 10^{-03}$	$3.72 \cdot 10^{-03}$	$9.36 \cdot 10^{-03}$	$6.42 \cdot 10^{-03}$
July	NA	$3.90 \cdot 10^{-03}$	$-6.09 \cdot 10^{-03}$	$-9.41 \cdot 10^{-03}$	$4.04 \cdot 10^{-03}$	NA	$3.79 \cdot 10^{-03}$	$7.12 \cdot 10^{-03}$	$3.86 \cdot 10^{-03}$
August	NA	$-4.07 \cdot 10^{-03}$	NA	$6.44 \cdot 10^{-03}$	$3.60 \cdot 10^{-03}$	NA	$2.22 \cdot 10^{-03}$	$8.33 \cdot 10^{-03}$	$1.03 \cdot 10^{-02}$
September	$5.97 \cdot 10^{-03}$	$5.64 \cdot 10^{-04}$	NA	$3.90 \cdot 10^{-03}$	$5.38 \cdot 10^{-03}$	$-1.03 \cdot 10^{-02}$	$-1.16 \cdot 10^{-02}$	$-2.29 \cdot 10^{-03}$	$1.37 \cdot 10^{-02}$
October	$4.99 \cdot 10^{-03}$	$4.06 \cdot 10^{-03}$	NA	$4.82 \cdot 10^{-03}$	$6.02 \cdot 10^{-03}$	$1.07 \cdot 10^{-03}$	$9.39 \cdot 10^{-04}$	$4.93 \cdot 10^{-03}$	$1.27 \cdot 10^{-02}$
November	$2.79 \cdot 10^{-03}$	$6.23 \cdot 10^{-03}$	NA	$6.60 \cdot 10^{-03}$	$6.15 \cdot 10^{-03}$	NA	$-5.91 \cdot 10^{-04}$	$7.62 \cdot 10^{-03}$	$6.58 \cdot 10^{-03}$
December	NA	$-1.94 \cdot 10^{-04}$	NA	$4.03 \cdot 10^{-03}$	$4.02 \cdot 10^{-04}$	$-2.08 \cdot 10^{-03}$	$2.89 \cdot 10^{-03}$	$1.51 \cdot 10^{-02}$	$8.75 \cdot 10^{-03}$
Season	**BSh**	**BSk**	**BWh**	**BWk**	**Cfa**	**Csa**	**Csb**	**Dfa**	**Dfb**
Winter	NA	$-2.42 \cdot 10^{-03}$	NA	$5.21 \cdot 10^{-03}$	$7.86 \cdot 10^{-03}$	$3.07 \cdot 10^{-03}$	$1.86 \cdot 10^{-03}$	$1.25 \cdot 10^{-02}$	$1.61 \cdot 10^{-02}$
Spring	NA	$8.17 \cdot 10^{-03}$	NA	NA	$1.51 \cdot 10^{-02}$	$1.43 \cdot 10^{-03}$	$2.24 \cdot 10^{-02}$	$1.54 \cdot 10^{-02}$	$1.97 \cdot 10^{-02}$
Summer	$8.57 \cdot 10^{-03}$	$3.54 \cdot 10^{-03}$	NA	$1.63 \cdot 10^{-02}$	$7.05 \cdot 10^{-03}$	$1.42 \cdot 10^{-02}$	$-5.59 \cdot 10^{-04}$	$1.49 \cdot 10^{-02}$	$1.82 \cdot 10^{-02}$
Fall	$1.25 \cdot 10^{-02}$	$6.46 \cdot 10^{-03}$	NA	$6.54 \cdot 10^{-03}$	$1.36 \cdot 10^{-02}$	$-5.43 \cdot 10^{-03}$	$-7.12 \cdot 10^{-03}$	$5.00 \cdot 10^{-03}$	$1.64 \cdot 10^{-02}$

Table 2.2 Mean slope value for extreme precipitation events [number of extremes/years of record] of each Koeppen-Geiger region, which are significant at the 95th percentile. The total number of significant stations is shown in parenthesis in Table 2.1 and NA values indicate no significant stations for reference.

the mean slope values for each region. The average winter slope value range is most negative in the arid zone with $-2.42 \cdot 10^{-03}$ [number of extremes/year] and highest in the snow zone with $1.61 \cdot 10^{-02}$ [number of extremes/year]. During the spring, the average slope range occurs within the warm temperate zone. The average slope values are $1.43 \cdot 10^{-03}$ [number of extremes/year] to $2.24 \cdot 10^{-02}$ [number of extremes/year]. The summer average slope values range from $-5.59 \cdot 10^{-04}$ [number of extremes/year] within the warm temperate zone and $1.82 \cdot 10^{-02}$ [number of extremes/year] within the snow zone. The average fall slope values are all positive and vary from the low end occurring in the warm temperate zone at $-7.12 \cdot 10^{-03}$ [number of extremes/year] to the high end occurring in the snow zone at $1.64 \cdot 10^{-02}$ [number of extremes/year] (Table 2.2).

The **arid zone** only shows trends for the BSh (summer and fall), BSk (winter, spring, summer and fall), and BWk regions (winter, summer and fall). For this zone all slope values are positive, indicating a gain of extremes over all seasons, excluding BSk winter. The BSk winter is the only arid zone region losing extreme precipitation and the rate is $-2.42 \cdot 10^{-03}$. The average slope value that indicates the smallest gain of extreme precipitation events occur within the BSh region (1 significant station) during the fall and is $8.57 \cdot 10^{-03}$ [number of extremes/year]. The average slope value indicating the largest gain of extreme precipitation is $1.63 \cdot 10^{-02}$ [number of extremes/year] and is found during the summer within the BWk region (1 significant station).

The **warm temperate zone** contains many significant trends for all seasons and majority of the significant trends are located within the Cfa region. The average slope value that indicates the greatest loss of extreme precipitation events occurs within the Csb region (5 significant stations) during the fall and is $-7.12 \cdot 10^{-03}$ [number of extremes/year]. The average slope value indicating the opposite trend, a gain of

Month	**BSh**	**BSk**	**BWh**	**BWk**	**Cfa**	**Csa**	**Csb**	**Dfa**	**Dfb**
January	26.67 (2)	12.81 (40)	NA	19.44 (1)	19.87 (68)	18.56 (5)	12.86 (32)	9.44 (13)	6.53 (32)
February	28.89 (3)	15.46 (43)	27.22 (1)	20.00 (2)	19.51 (59)	18.56 (5)	15.21 (27)	11.69 (29)	6.73 (68)
March	30.83 (2)	20.32 (68)	30.56 (1)	23.64 (6)	25.31 (66)	22.96 (3)	19.56 (15)	18.21 (13)	13.15 (54)
April	35.28 (2)	26.31 (37)	NA	27.96 (3)	28.35 (100)	27.89 (5)	23.08 (22)	24.54 (19)	21.25 (41)
May	37.59 (3)	31.14 (45)	39.44 (1)	35.09 (6)	31.67 (155)	31.81 (4)	27.04 (21)	29.44 (27)	26.73 (26)
June	NA	34.91 (36)	43.33 (1)	39.78 (5)	34.78 (155)	38.19 (4)	30.89 (19)	33.26 (46)	30.28 (44)
July	40.74 (3)	36.60 (60)	43.33 (3)	40.83 (4)	36.01 (129)	38.11 (5)	33.10 (26)	34.94 (77)	32.53 (63)
August	40.56 (2)	35.53 (51)	43.89 (2)	40.37 (3)	35.87 (113)	37.46 (7)	32.58 (28)	33.86 (74)	31.84 (59)
September	39.07 (3)	32.03 (44)	41.11 (1)	37.41 (3)	33.97 (158)	34.17 (4)	30.66 (32)	31.60 (51)	28.81 (49)
October	35.56 (1)	27.81 (34)	NA	29.44 (5)	29.68 (136)	31.25 (4)	25.31 (23)	26.25 (28)	23.39 (32)
November	32.22 (1)	19.88 (34)	30.00 (1)	24.63 (3)	24.72 (70)	22.22 (2)	19.08 (20)	19.14 (11)	14.57 (29)
December	28.61 (2)	15.83 (29)	24.44 (1)	20.00 (1)	19.58 (52)	17.36 (4)	15.72 (17)	11.18 (16)	7.94 (28)
Season	**BSh**	**BSk**	**BWh**	**BWk**	**Cfa**	**Csa**	**Csb**	**Dfa**	**Dfb**
Winter	27.50 (2)	14.53 (50)	NA	18.33 (2)	19.70 (71)	18.43 (6)	14.07 (28)	11.36 (29)	7.51 (66)
Spring	36.39 (2)	28.08 (52)	37.22 (1)	31.94 (6)	29.75 (151)	29.31 (4)	24.69 (27)	26.60 (25)	23.59 (45)
Summer	40.56 (3)	35.75 (69)	42.78 (3)	40.00 (5)	35.68 (153)	37.50 (6)	32.88 (39)	34.17 (87)	31.67 (77)
Fall	36.94 (4)	29.42 (58)	NA	33.33 (6)	31.72 (195)	31.67 (4)	27.37 (38)	28.59 (43)	25.46 (68)

Table 2.3 Mean magnitude threshold for an extreme maximum temperature [°C] to occur within each Koeppen-Geiger region. The parenthesis indicate the number of significant stations in the climate region and NA values indicate no significant stations for reference. All values shown are significant at the 95th percentile.

extremes, also occurs within the Csb region (15 significant station) during the spring and is $2.24 \cdot 10^{-02}$ [number of extremes/year].

The **snow zone** contains the largest positive slope values, that is a gain in extreme precipitation event for the past 100 years. All significant trends are positive for this region. The smallest average positive trend occurs during winter within the Dfa region at a rate of $5.00 \cdot 10^{-03}$ [number of extremes/year] (27 significant stations). The average slope value indicating the largest gain in extreme precipitation events occurs in the summer within the Dfb region at a rate of $1.82 \cdot 10^{-02}$ [number of extremes/year] (35 significant stations).

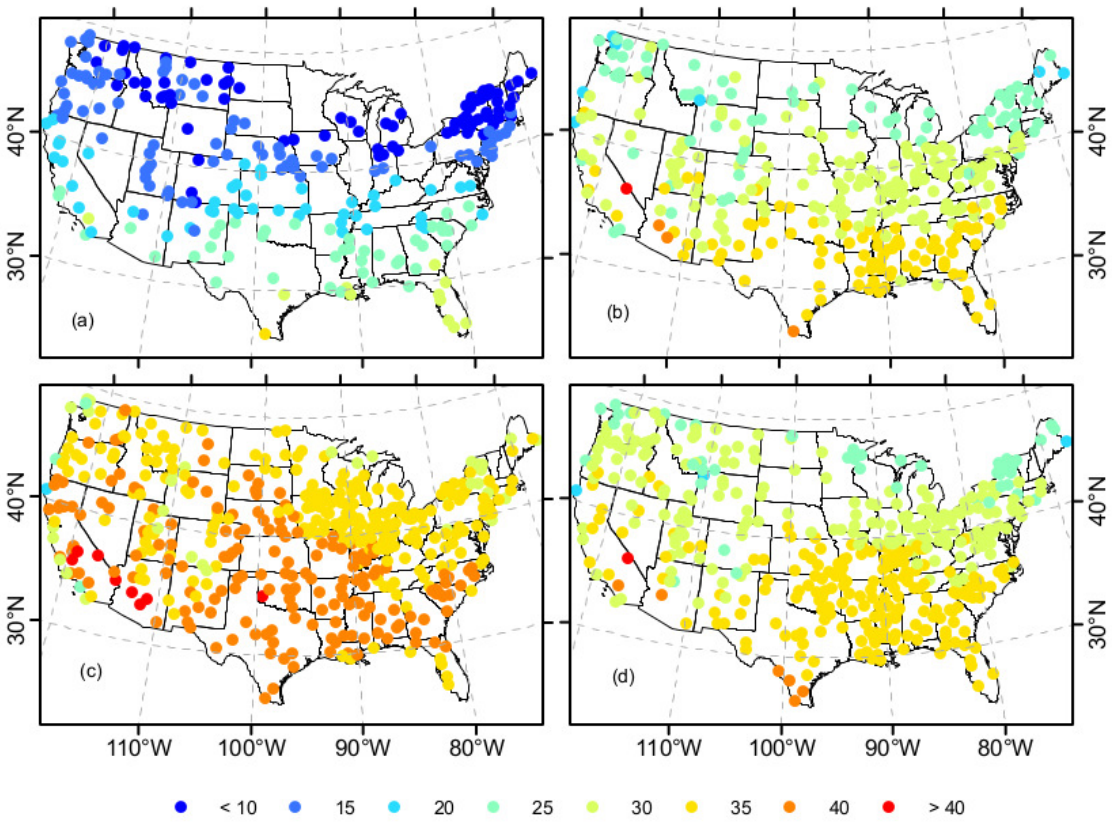

Figure 2.4 Magnitude threshold for an extreme maximum temperature event to occur [°C]. (a) Winter (206 significant stations), (b) Spring (263 significant stations), (c) Summer (376 significant stations) and (d) Fall (362 significant stations). Significant stations indicated by a Mann-Kendall p-value ≤ 0.05.

2.4.3 Extreme Maximum Temperature

Seasonal Variation in Magnitude

The threshold for extreme daily maximum temperate ranges from $\leq$10 °C to $\geq$40 °C for all seasons (Figure 2.4). Summer naturally exhibits higher thresholds of maximum temperature than does winter for a majority of the US, an extreme heat event coincides with temperatures in the range of $30 - 40$ °C. Lower threshold values are present in the northern portion of the US (Dfa, Dfb and northern Csb). For all seasons, the highest threshold levels are isolated to the desert southwest (BSh, southern BSk, BWh and BWk). The mean monthly magnitude threshold for each climate zone can be found in Table 2.3. For winter the average threshold range varies between the snow zone at the low end with 7.51 °C to the high end in the arid zone at 27.50 °C. During the spring season the threshold increases in range and occurs within the snow (low end) to arid (high end), and are 23.59 °C and 36.39 °C respectively. For the summer the average threshold for extreme daily maximum temperature lowest at 31.67 °C and occurs within the snow zone, while the highest occurs within the arid at 42.78 °C. The fall average threshold range is 25.46 °C occurring in the snow to 36.94 °C occurring in the arid zone (Table 2.3).

The **arid zone** has the highest extreme maximum temperature thresholds and is valid within all regions based on significance, excluding the BWh region (winter and fall). The lowest threshold for an extreme temperature event to occur is found in the BSk region during the winter and is 14.53 °C (50 significant stations). The highest threshold for an extreme temperature event to occur in the arid zone is found in the BWh region during the summer and is 42.78 °C (3 significant stations).

The **warm temperate zone** is similar to the arid zone in terms of seasonality but the threshold variation is not as large. The highest threshold for an extreme heat

event is 37.50 °C which occurs in the Csa region during the summer (6 significant stations). The lowest threshold for an extreme heat event can be found in the Csb region during the winter at 14.07 °C (28 significant stations).

The **snow zone** has a lower threshold for extreme heat events. An extreme heat event can occur at as low as 7.51 °C during the winter within the Dfb region (66 significant stations). The hottest threshold value for an extreme heat event to occur in the snow zone can be found in the Dfa region during the summer. That value is 34.17 °C (87 significant stations).

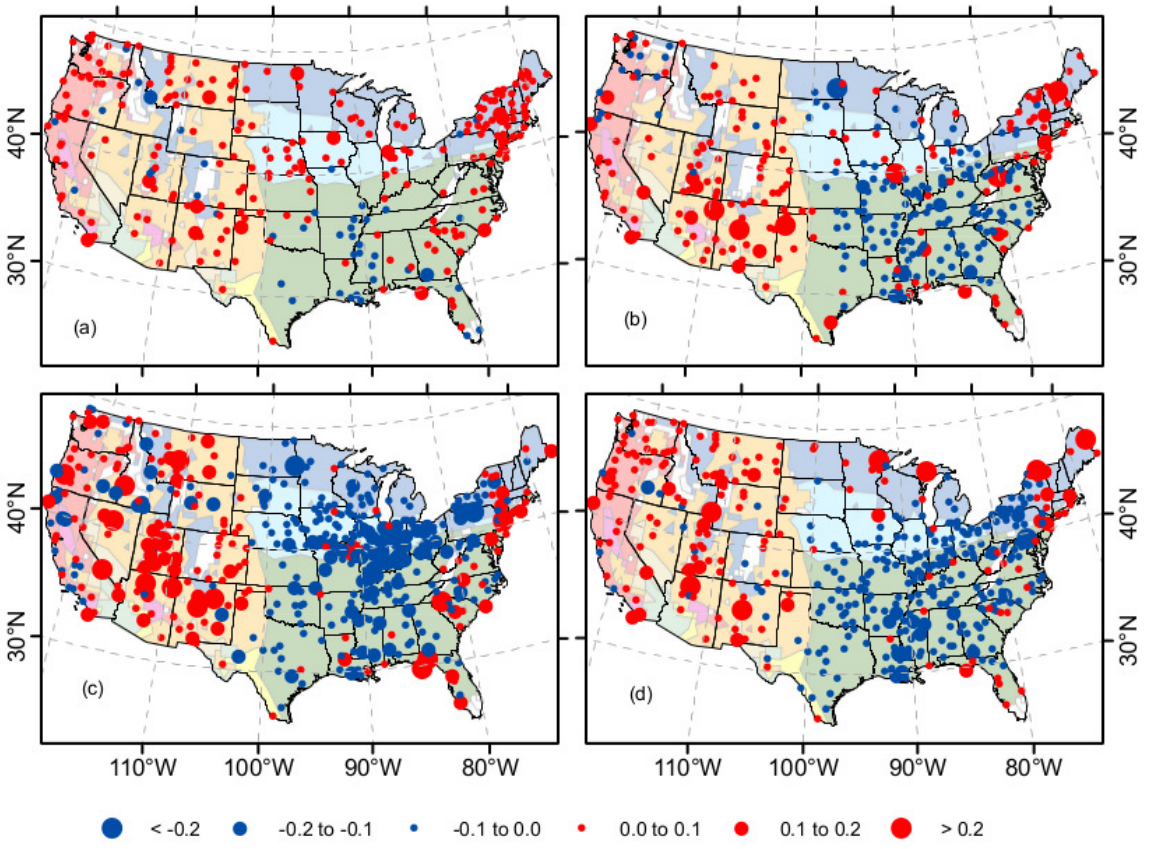

Figure 2.5 Slope of extreme maximum temperature events [number of extremes/year]. (a) Winter (206 significant stations), (b) Spring 263 significant stations), (c) Summer (376 significant stations) and (d) Fall (362 significant stations). Significant stations indicated by a Mann-Kendall p-value ≤ 0.05. Koeppen-Geiger classification are shown faded in bottom layer

Month	BSh	BSk	BWh	BWk	Cfa	Csa	Csb	Dfa	Dfb
January	$2.20 \cdot 10^{-02}$	$2.79 \cdot 10^{-02}$	NA	$2.49 \cdot 10^{-02}$	$-7.57 \cdot 10^{-03}$	$3.11 \cdot 10^{-02}$	$2.53 \cdot 10^{-02}$	$4.92 \cdot 10^{-03}$	$1.55 \cdot 10^{-02}$
February	$6.29 \cdot 10^{-03}$	$2.47 \cdot 10^{-02}$	$1.74 \cdot 10^{-02}$	$1.69 \cdot 10^{-02}$	$1.56 \cdot 10^{-02}$	$2.82 \cdot 10^{-02}$	$2.20 \cdot 10^{-02}$	$1.97 \cdot 10^{-02}$	$2.39 \cdot 10^{-02}$
March	$4.89 \cdot 10^{-04}$	$3.11 \cdot 10^{-02}$	$1.80 \cdot 10^{-02}$	$2.67 \cdot 10^{-02}$	$-3.39 \cdot 10^{-03}$	$1.50 \cdot 10^{-02}$	$6.49 \cdot 10^{-03}$	$2.13 \cdot 10^{-02}$	$2.45 \cdot 10^{-02}$
April	$2.16 \cdot 10^{-02}$	$2.38 \cdot 10^{-02}$	NA	$1.38 \cdot 10^{-02}$	$8.02 \cdot 10^{-03}$	$2.16 \cdot 10^{-02}$	$7.63 \cdot 10^{-03}$	$2.93 \cdot 10^{-02}$	$2.14 \cdot 10^{-02}$
May	$2.86 \cdot 10^{-02}$	$2.97 \cdot 10^{-02}$	$3.12 \cdot 10^{-02}$	$4.52 \cdot 10^{-02}$	$-2.12 \cdot 10^{-02}$	$2.44 \cdot 10^{-02}$	$2.81 \cdot 10^{-02}$	$3.49 \cdot 10^{-03}$	$3.08 \cdot 10^{-03}$
June	NA	$2.24 \cdot 10^{-02}$	$2.91 \cdot 10^{-02}$	$2.36 \cdot 10^{-02}$	$-2.64 \cdot 10^{-02}$	$-1.69 \cdot 10^{-02}$	$8.30 \cdot 10^{-03}$	$-2.50 \cdot 10^{-02}$	$-7.95 \cdot 10^{-05}$
July	$1.20 \cdot 10^{-02}$	$2.57 \cdot 10^{-02}$	$3.63 \cdot 10^{-02}$	$4.75 \cdot 10^{-02}$	$-1.75 \cdot 10^{-02}$	$-2.16 \cdot 10^{-02}$	$2.16 \cdot 10^{-02}$	$-3.23 \cdot 10^{-02}$	$-7.99 \cdot 10^{-03}$
August	$-4.77 \cdot 10^{-03}$	$1.02 \cdot 10^{-02}$	$4.51 \cdot 10^{-02}$	$3.59 \cdot 10^{-02}$	$-4.17 \cdot 10^{-03}$	$-3.49 \cdot 10^{-03}$	$2.50 \cdot 10^{-02}$	$-2.08 \cdot 10^{-02}$	$-1.43 \cdot 10^{-02}$
September	$1.32 \cdot 10^{-02}$	$1.86 \cdot 10^{-02}$	$2.39 \cdot 10^{-02}$	$4.51 \cdot 10^{-02}$	$-2.70 \cdot 10^{-02}$	$2.75 \cdot 10^{-02}$	$1.81 \cdot 10^{-02}$	$-2.30 \cdot 10^{-02}$	$2.89 \cdot 10^{-04}$
October	$5.17 \cdot 10^{-03}$	$2.43 \cdot 10^{-02}$	NA	$2.38 \cdot 10^{-02}$	$-2.20 \cdot 10^{-02}$	$-3.55 \cdot 10^{-02}$	$-4.90 \cdot 10^{-03}$	$-1.68 \cdot 10^{-02}$	$-9.02 \cdot 10^{-03}$
November	$1.18 \cdot 10^{-02}$	$2.01 \cdot 10^{-02}$	$-2.59 \cdot 10^{-02}$	$2.75 \cdot 10^{-02}$	$5.83 \cdot 10^{-03}$	$2.71 \cdot 10^{-02}$	$-9.19 \cdot 10^{-03}$	$4.51 \cdot 10^{-02}$	$2.85 \cdot 10^{-02}$
December	$2.25 \cdot 10^{-03}$	$1.21 \cdot 10^{-02}$	$-2.38 \cdot 10^{-02}$	$1.71 \cdot 10^{-02}$	$1.38 \cdot 10^{-02}$	$2.36 \cdot 10^{-02}$	$-1.41 \cdot 10^{-02}$	$1.24 \cdot 10^{-02}$	$2.12 \cdot 10^{-02}$
Season	**BSh**	**BSk**	**BWh**	**BWk**	**Cfa**	**Csa**	**Csb**	**Dfa**	**Dfb**
Winter	$5.15 \cdot 10^{-02}$	$4.99 \cdot 10^{-02}$	NA	$4.31 \cdot 10^{-02}$	$1.39 \cdot 10^{-02}$	$6.69 \cdot 10^{-02}$	$4.18 \cdot 10^{-02}$	$4.09 \cdot 10^{-02}$	$4.76 \cdot 10^{-02}$
Spring	$5.59 \cdot 10^{-02}$	$5.75 \cdot 10^{-02}$	$5.91 \cdot 10^{-02}$	$6.21 \cdot 10^{-02}$	$-1.99 \cdot 10^{-02}$	$6.14 \cdot 10^{-02}$	$2.87 \cdot 10^{-02}$	$2.52 \cdot 10^{-02}$	$2.68 \cdot 10^{-02}$
Summer	$2.08 \cdot 10^{-02}$	$5.44 \cdot 10^{-02}$	$8.18 \cdot 10^{-02}$	$1.06 \cdot 10^{-01}$	$-4.40 \cdot 10^{-02}$	$-3.53 \cdot 10^{-02}$	$4.34 \cdot 10^{-02}$	$-6.82 \cdot 10^{-02}$	$-3.26 \cdot 10^{-02}$
Fall	$4.11 \cdot 10^{-03}$	$4.41 \cdot 10^{-02}$	NA	$7.30 \cdot 10^{-02}$	$-5.31 \cdot 10^{-02}$	$7.07 \cdot 10^{-02}$	$4.80 \cdot 10^{-02}$	$-3.31 \cdot 10^{-02}$	$2.03 \cdot 10^{-02}$

Table 2.4 Mean slope value for extreme maximum temperature events [number of extremes/years of record] of each Koeppen-Geiger region, which are significant at the 95th percentile. The total number of significant stations is shown in parenthesis in Table 2.3 and NA values indicate no significant stations for reference.

Seasonal Variation in Slope

Slope values for extreme maximum temperature range from $\leq$ -0.2 to $\geq$ 0.2 and are shown in Figure 2.5. The frequency of extreme heat events in the past 100 years has increased/decreased by roughly 20 events. Table 2.4 gives the mean monthly slope value for each climate region. In the winter the slope value are all positive and range from low to high within the snow to the warm temperate zone at $4.09 \cdot 10^{-02}$ [number of extremes/year] to $6.69 \cdot 10^{-02}$ [number of extremes/year]. During the spring the lowest value can be found in the warm temperature region at $-1.99 \cdot 10^{-02}$ [number of extremes/year], while the highest value is found within the arid zones at $\cdot 10^{-02}$ [number of extremes/year]. Summer values range from $-6.82 \cdot 10^{-02}$ [number of extremes/year] to $1.06 \cdot 10^{-01}$ [number of extremes/year] within the snow and

arid respectively. For the fall the slope value the lowest slope is found in he warm temperate zone at $-5.31 \cdot 10^{-02}$ [number of extremes/year], and the highest within the arid zone at $7.30 \cdot 10^{-02}$ [number of extremes/year].

The **arid zone** zone contains positive slope values for all seasons, thus this region has only seen a gain in extreme heat events. The slope values range from lowest being found in the BSh region during summer at $2.08 \cdot 10^{-02}$ [number of extremes/year] (3 significant stations) and the highest being found during the BWk region summer at $1.06 \cdot 10^{-01}$ [number of extremes/year] (5 significant stations).

The **warm temperate zone** shows different trends for the western US warm temperate (Csa and Csb region) versus the eastern US warm temperate (Cfa region). The lowest overall slope value is found in the fall within the Cfa region and is $-5.31 \cdot 10^{-02}$ [number of extremes/year] (195 significant stations), while the highest is found in the fall within the Csa region at $7.07 \cdot 10^{-02}$ [number of extremes/year] (4 significant stations).

The **snow zone** holds the lowest slope value for all of the US. This value can be found in the Dfa region during the summer and is $-6.82 \cdot 10^{-02}$ [number of extremes/year] (87 significant stations). The highest value can be found in the Dfb region during the winter at $4.76 \cdot 10^{-02}$ [number of extremes/year] (66 significant stations).

2.4.4 Extreme Minimum Temperature

Seasonal Variation in Magnitude

Magnitude values for all months are shown in Figure 2.6, and range from $\leq -20\,^{\circ}\mathrm{C}$ to $\geq 20\,^{\circ}\mathrm{C}$. The higher threshold values are present in all coastal regions exceed the continental stations thresholds for the majority of the seasons. Summer is the

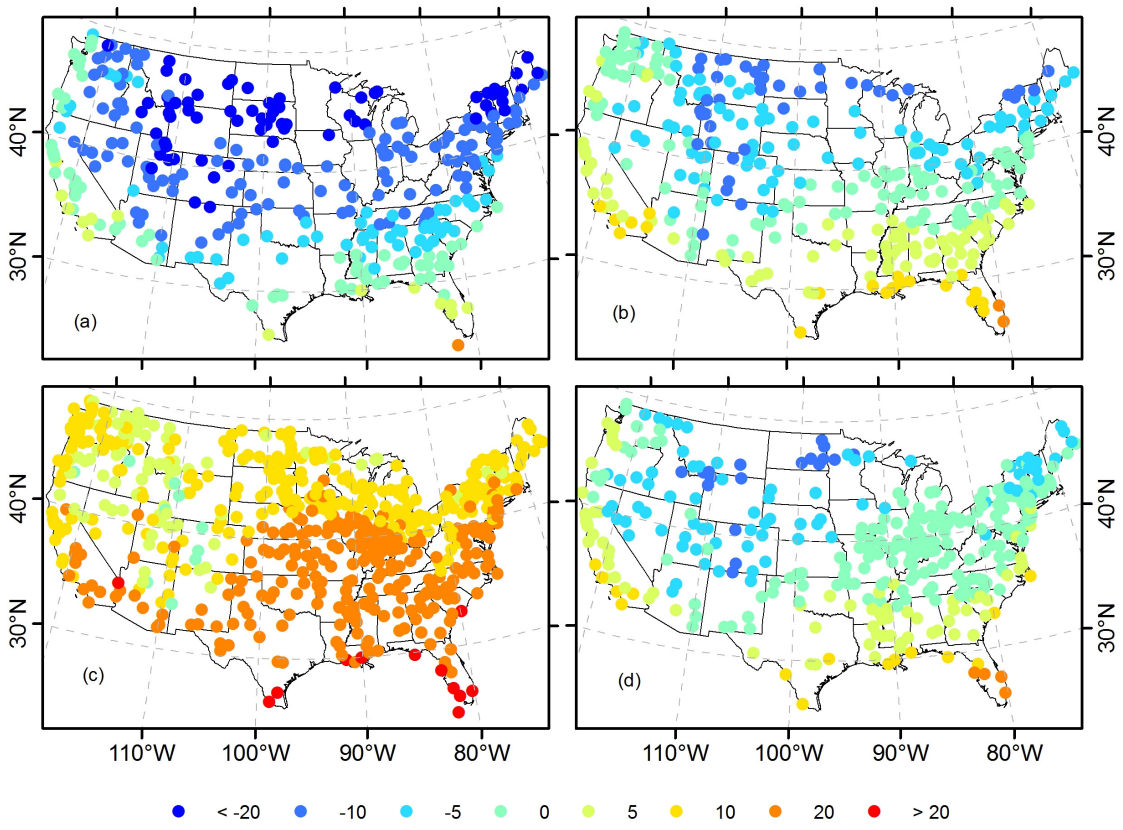

Figure 2.6 Magnitude threshold for an extreme minimum temperature event to occur [°C]. (a) Winter (325 significant stations), (b) Spring (317 significant stations), (c) Summer (564 significant stations) and (d) Fall (346 significant stations). Significant stations indicated by a Mann-Kendall p-value ≤ 0.05.

Month	**BSh**	**BSk**	**BWh**	**BWk**	**Cfa**	**Csa**	**Csb**	**Dfa**	**Dfb**
January	−2.41 (3)	−14.10 (41)	−1.78 (5)	−10.83 (2)	−7.38 (94)	−5.69 (4)	−6.25 (25)	−21.43 (14)	−24.85 (40)
February	1.67 (1)	−13.18 (34)	−0.07 (4)	−5.28 (2)	−6.38 (63)	1.11 (1)	−4.82 (22)	−20.04 (30)	−22.29 (82)
March	0.93 (3)	−8.94 (42)	3.56 (5)	−4.72 (4)	−2.49 (71)	-1.11 (3)	−2.07 (34)	−11.07 (10)	−14.15 (35)
April	10.56 (1)	−2.61 (33)	7.22 (3)	1.67 (2)	2.21 (127)	2.92 (4)	−0.48 (38)	−3.16 (37)	−5.58 (62)
May	9.44 (1)	2.10 (50)	11.56 (5)	5.56 (4)	7.67 (117)	6.67 (2)	2.66 (38)	2.25 (60)	−0.23 (86)
June	14.07 (3)	7.07 (65)	16.33 (5)	10.83 (4)	13.31 (135)	7.41 (6)	5.31 (51)	8.62 (97)	5.02 (92)
July	19.72 (2)	10.52 (68)	21.56 (5)	12.92 (4)	16.26 (132)	10.11 (5)	7.40 (58)	11.75 (84)	8.51 (107)
August	16.67 (1)	9.41 (61)	20.78 (5)	11.39 (4)	15.44 (125)	9.44 (6)	6.97 (53)	10.53 (77)	7.36 (105)
September	17.22 (1)	4.04 (55)	15.44 (5)	5.56 (4)	10.23 (102)	5.83 (6)	3.97 (43)	3.78 (35)	1.48 (86)
October	9.44 (2)	−2.22 (48)	7.36 (4)	3.06 (2)	2.44 (109)	3.06 (4)	0.73 (31)	−1.91 (25)	−3.78 (58)
November	4.44 (1)	−7.69 (22)	0.83 (4)	−5.74 (3)	−2.89 (122)	−1.94 (2)	−2.90 (23)	−6.96 (28)	−9.57 (45)
December	−1.67 (3)	−11.98 (32)	−1.94 (4)	−7.22 (1)	−6.55 (81)	−6.11 (1)	−4.79 (19)	−16.42 (18)	−18.80 (60)
Season	**BSh**	**BSk**	**BWh**	**BWk**	**Cfa**	**Csa**	**Csb**	**Dfa**	**Dfb**
Winter	−2.04 (3)	−13.98 (59)	−1.11 (5)	−11.78 (5)	−6.68 (109)	−6.00 (5)	−5.87 (31)	−20.42 (29)	−22.80 (79)
Spring	4.63 (3)	−5.83 (63)	5.78 (5)	−1.00 (5)	0.48 (126)	2.22 (2)	−1.12 (42)	−6.33 (20)	−9.25 (51)
Summer	16.48 (3)	8.33 (80)	18.56 (5)	11.44 (5)	14.79 (175)	8.49 (7)	6.03 (60)	10.19 (106)	6.73 (123)
Fall	6.67 (2)	−4.94 (47)	3.75 (4)	−2.22 (4)	0.23 (140)	1.56 (5)	−0.57 (31)	−3.96 (41)	−5.67 (72)

Table 2.5 Mean magnitude threshold for an extreme minimum temperature [°C] to occur within each Koeppen-Geiger region. The parenthesis indicate the number of significant stations in the climate region and NA values indicate no significant stations for reference. All values shown are significant at the 95th percentile.

exception, where higher threshold values are present throughout the whole US. The mean magnitude for each region can be found in Table 2.5. During the winter months the lowest threshold for an extreme cold event to occur is found in the snow zone and is −22.80 °C. The highest threshold for extreme winter cold is found in the arid zone at −1.11 °C. During the spring the lowest threshold is found in the snow zone at −9.25 °C and the highest in the arid zone at 5.78 °C. For an extreme cold event to occur in the summer the low end threshold is 6.03 °C in the warm temperate zone and 18.56 °C in the arid zone. Fall extreme cold event thresholds range from −5.67 °C in the snow zone to 6.67 °C in the arid zone (Table 2.5).

The **arid zone** has some of the warmest thresholds for an extreme cold event. The lowest threshold in this zone occurs within the BSk region during the spring at −13.98 °C (59 significant stations) while the highest threshold occurs within the BWh region during the summer at 18.56 °C (5 significant stations).

The **warm temperate zone** thresholds are similar to the arid zone but with less range. The lowest temperature for an extreme cold event to occur is −6.68 °C in the Cfa region during the winter (109 significant stations) and the warmest is 14.79 °C in the Cfa region during the summer (175 significant stations).

The **snow zone** contains the coldest threshold for extreme cold events. The coldest threshold for the US is located in the Dfb region during the winter at −22.80 °C (79 significant stations). The warmest threshold for this zone occurs in the Dfa region during the summer and is 10.19 °C (106 significant stations).

Seasonal Differences in Slope

Slope values range from ≤ -0.2 to ≥ 0.2 and are shown in Figure 2.7. Some areas show extreme daily cold events increasing or decreasing by roughly 20 events in the past 100 years. Note that negative slope values correspond to fewer extreme cold events.

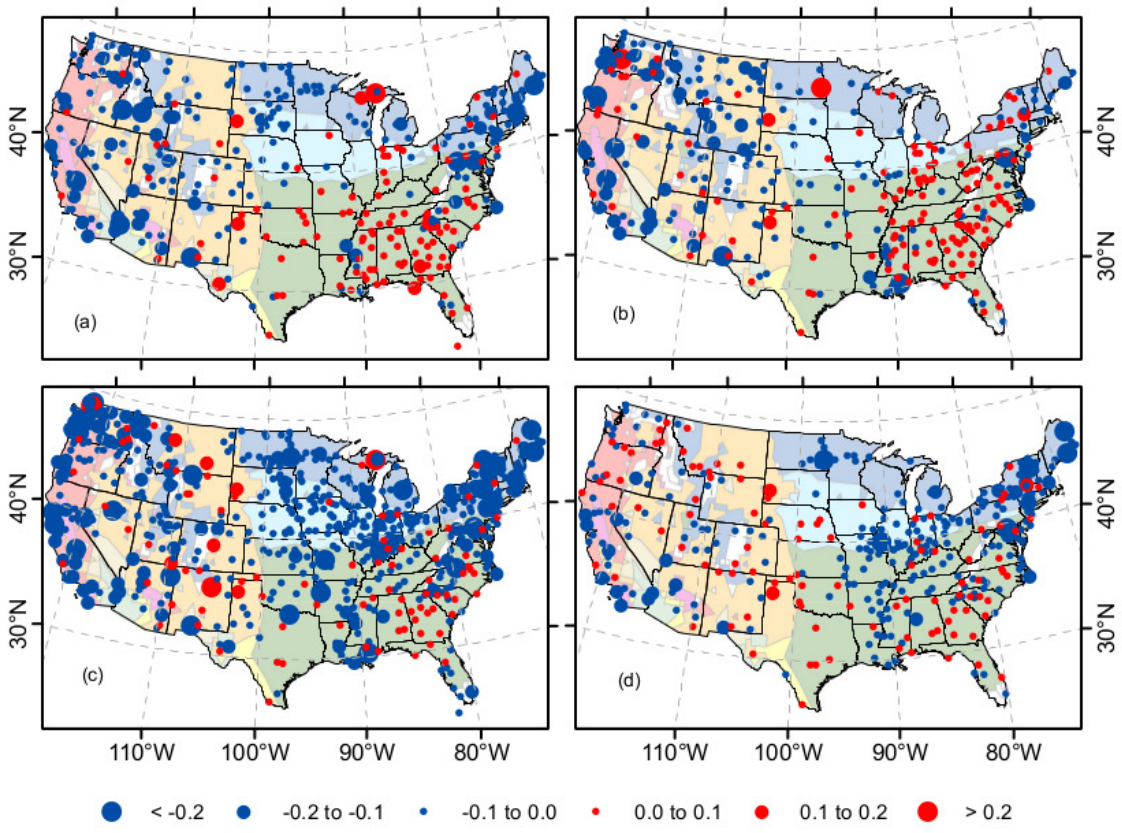

Figure 2.7 Slope of extreme minimum temperature events [number of extremes/year]. (a) Winter (325 significant stations), (b) Spring (317 significant stations), (c) Summer (564 significant stations) and (d) Fall (346 significant stations). Significant are stations based on the Mann-Kendall P-value $\leq$ 0.05. Koeppen-Geiger classification are shown faded in bottom layer.

Month	BSh	BSk	BWh	BWk	Cfa	Csa	Csb	Dfa	Dfb
January	$-1.17 \cdot 10^{-02}$	$-3.55 \cdot 10^{-02}$	$-6.10 \cdot 10^{-02}$	$-8.08 \cdot 10^{-02}$	$2.31 \cdot 10^{-02}$	$-4.08 \cdot 10^{-02}$	$-3.73 \cdot 10^{-02}$	$1.90 \cdot 10^{-02}$	$-1.28 \cdot 10^{-02}$
February	$1.78 \cdot 10^{-02}$	$-2.12 \cdot 10^{-02}$	$-3.53 \cdot 10^{-02}$	$-4.15 \cdot 10^{-02}$	$-8.22 \cdot 10^{-03}$	$-2.08 \cdot 10^{-02}$	$-2.19 \cdot 10^{-02}$	$-1.07 \cdot 10^{-02}$	$-2.57 \cdot 10^{-02}$
March	$-9.41 \cdot 10^{-03}$	$-2.93 \cdot 10^{-02}$	$-4.71 \cdot 10^{-02}$	$-2.93 \cdot 10^{-02}$	$7.09 \cdot 10^{-03}$	$-4.66 \cdot 10^{-02}$	$-2.81 \cdot 10^{-02}$	$5.48 \cdot 10^{-03}$	$-1.60 \cdot 10^{-02}$
April	$2.10 \cdot 10^{-02}$	$-5.76 \cdot 10^{-03}$	$-4.57 \cdot 10^{-02}$	$-2.79 \cdot 10^{-02}$	$8.02 \cdot 10^{-04}$	$2.03 \cdot 10^{-02}$	$-1.25 \cdot 10^{-02}$	$-1.37 \cdot 10^{-02}$	$-1.93 \cdot 10^{-02}$
May	$-3.42 \cdot 10^{-02}$	$-5.37 \cdot 10^{-03}$	$-4.43 \cdot 10^{-02}$	$-2.44 \cdot 10^{-02}$	$1.95 \cdot 10^{-04}$	$-2.78 \cdot 10^{-02}$	$-1.57 \cdot 10^{-02}$	$-2.15 \cdot 10^{-02}$	$-1.57 \cdot 10^{-02}$
June	$-3.26 \cdot 10^{-02}$	$-1.73 \cdot 10^{-02}$	$-4.41 \cdot 10^{-02}$	$-3.27 \cdot 10^{-02}$	$-1.81 \cdot 10^{-02}$	$-3.09 \cdot 10^{-02}$	$-3.49 \cdot 10^{-02}$	$-2.06 \cdot 10^{-02}$	$-2.55 \cdot 10^{-02}$
July	$-2.85 \cdot 10^{-02}$	$-2.85 \cdot 10^{-02}$	$-4.43 \cdot 10^{-02}$	$-3.18 \cdot 10^{-02}$	$-1.84 \cdot 10^{-02}$	$-3.07 \cdot 10^{-02}$	$-3.80 \cdot 10^{-02}$	$-2.23 \cdot 10^{-02}$	$-2.92 \cdot 10^{-02}$
August	$-6.26 \cdot 10^{-02}$	$-3.01 \cdot 10^{-02}$	$-4.00 \cdot 10^{-02}$	$-3.62 \cdot 10^{-02}$	$-1.86 \cdot 10^{-02}$	$-4.31 \cdot 10^{-02}$	$-4.61 \cdot 10^{-02}$	$-2.20 \cdot 10^{-02}$	$-3.23 \cdot 10^{-02}$
September	$2.41 \cdot 10^{-02}$	$-2.61 \cdot 10^{-02}$	$-4.70 \cdot 10^{-02}$	$-2.57 \cdot 10^{-02}$	$-9.68 \cdot 10^{-04}$	$-3.25 \cdot 10^{-02}$	$-3.39 \cdot 10^{-02}$	$-1.51 \cdot 10^{-02}$	$-2.81 \cdot 10^{-02}$
October	$3.53 \cdot 10^{-03}$	$-6.41 \cdot 10^{-03}$	$-5.20 \cdot 10^{-02}$	$-2.93 \cdot 10^{-02}$	$2.69 \cdot 10^{-03}$	$-2.73 \cdot 10^{-02}$	$-1.20 \cdot 10^{-02}$	$-6.84 \cdot 10^{-03}$	$-1.29 \cdot 10^{-02}$
November	$1.95 \cdot 10^{-02}$	$-2.75 \cdot 10^{-03}$	$-4.66 \cdot 10^{-02}$	$-1.98 \cdot 10^{-02}$	$-1.56 \cdot 10^{-02}$	$-1.73 \cdot 10^{-02}$	$-1.27 \cdot 10^{-02}$	$-1.86 \cdot 10^{-02}$	$-2.25 \cdot 10^{-02}$
December	$-9.52 \cdot 10^{-03}$	$-1.40 \cdot 10^{-02}$	$-5.14 \cdot 10^{-02}$	$1.93 \cdot 10^{-02}$	$-4.31 \cdot 10^{-03}$	$1.36 \cdot 10^{-02}$	$-1.11 \cdot 10^{-02}$	$-1.17 \cdot 10^{-02}$	$-3.05 \cdot 10^{-02}$
Season	**BSh**	**BSk**	**BWh**	**BWk**	**Cfa**	**Csa**	**Csb**	**Dfa**	**Dfb**
Winter	$-1.99 \cdot 10^{-02}$	$-6.33 \cdot 10^{-02}$	$-1.45 \cdot 10^{-01}$	$-7.56 \cdot 10^{-02}$	$1.81 \cdot 10^{-02}$	$-7.54 \cdot 10^{-02}$	$-6.54 \cdot 10^{-02}$	$-1.79 \cdot 10^{-02}$	$-4.88 \cdot 10^{-02}$
Spring	$-1.74 \cdot 10^{-02}$	$-5.06 \cdot 10^{-02}$	$-1.14 \cdot 10^{-01}$	$-6.17 \cdot 10^{-02}$	$1.31 \cdot 10^{-02}$	$-1.01 \cdot 10^{-01}$	$-5.03 \cdot 10^{-02}$	$1.43 \cdot 10^{-02}$	$-2.66 \cdot 10^{-02}$
Summer	$-6.00 \cdot 10^{-02}$	$-4.65 \cdot 10^{-02}$	$-1.23 \cdot 10^{-01}$	$-5.80 \cdot 10^{-02}$	$-4.62 \cdot 10^{-02}$	$-7.64 \cdot 10^{-02}$	$-9.23 \cdot 10^{-02}$	$-5.43 \cdot 10^{-02}$	$-7.31 \cdot 10^{-02}$
Fall	$1.93 \cdot 10^{-02}$	$-1.35 \cdot 10^{-02}$	$-1.14 \cdot 10^{-01}$	$-4.50 \cdot 10^{-02}$	$-1.97 \cdot 10^{-02}$	$-5.46 \cdot 10^{-02}$	$-2.79 \cdot 10^{-02}$	$-2.64 \cdot 10^{-02}$	$-4.99 \cdot 10^{-02}$

Table 2.6 Mean slope value for extreme minimum temperature events [number of extremes/years of record] of each Koeppen-Geiger region, which are significant at the 95th percentile. The total number of significant stations is shown in parenthesis in Table 2.5 and NA values indicate no significant stations for reference.

The summer season has roughly double the amount of significant stations than other months, which illustrates a strong trend in summer extreme minimum temperatures. Table 2.6 gives the mean monthly slope changes for extreme cold events based on climate region. For winter the trend in extreme cold events ranges from $-1.45 \cdot 10^{-01}$ [number of extremes/year] in the arid zone to $1.81 \cdot 10^{-02}$ [number of extremes/year] in the warm temperate zone. Spring thresholds range between $-1.14 \cdot 10^{-02}$ [number of extremes/year] to $1.31 \cdot 10^{-02}$ [number of extremes/year], within the arid and warm temperate respectively. During the summer the slope values for extreme cold events are all negative and range within the arid zone from the low end at $-1.23 \cdot 10^{-01}$ [number of extremes/year] to the high end in the snow zone at $-4.65 \cdot 10^{-02}$ [number of extremes/year]. Fall values range within the arid zone from $-1.14 \cdot 10^{-01}$ [number of extremes/year] to $1.93 \cdot 10^{-02}$ [number of extremes/year] (Table 2.6).

The **arid zone** has the smallest range of slope values with the largest values. The largest negative slope value for this zone occurs in the BWh region during the summer and is $-1.45 \cdot 10^{-01}$ [number of extremes/year] (5 significant stations) and is the most negative slope value overall. The most positive slope value can be found in the BSh region during the fall and is $1.93 \cdot 10^{-02}$ [number of extremes/year] (2 significant stations).

The **warm temperate zone** experiences are decrease in the frequency of extreme minimum temperature events, except for the winter and spring in the Cfa region. The Cfa region also contains the most positive trend which is found the winter and is $1.81 \cdot 10^{-02}$ (109 significant stations). The lowest slope value for this zone can be found in the Csa region during the spring and is $-1.01 \cdot 10^{-01}$ (2 significant stations).

The **snow zone** overall on average is losing extreme cold days. The largest negative trend in this zone occurs in the Dfb region during the summer and is $-7.31 \cdot 10^{-02}$ [number of extremes/year] (123 significant stations). The largest positive trend to oc-

cur in this zone is found in the Dfa region during the spring and is $1.43 \cdot 10^{-02}$ [number of extremes/year] (20 significant stations).

2.4.5 Climate Region Response

Figure 3.8 (extreme precipitation), figure 3.9 (extreme maximum temperature) and figure 3.10 (extreme minimum temperature) show the seasonal response in terms of slope and magnitude for extreme weather. All stations and all trends were used in this analysis and each Koeppen-Geiger region contains the following number of stations; 5 in BSh, 135 in BSk, 11 in BWh, 11 in BWk, 363 in Cfa, 16 in Csa, 78 in Csb, 166 in Dfa and 195 in Dfb. Extreme weather can be stratified by climate regime. Understanding how each Koeppen-Geiger region behaves can help quantify relative changes in past extreme events and show patterns within specific regions.

Extreme Precipitation

The **arid zone** slope distribution and threshold distribution can be found in Figure 2.8. The slope values have no seasonality present and a majority of the samples lies between -0.01 and 0.01[number of extremes/year]. In terms of magnitude there is a seasonal pattern. The BSk region contains a much larger variation in threshold needed for an extreme precipitation event to occur. Distributions of the threshold magnitudes for BSk, BWk and BWh regions are narrow but vary substantially, although they do not exceed 20 mm. It is important to note the separation between the BSh region and the other arid regions because with large shifts and variations seasonally.

The **warm temperate zone** slope distribution is found in Figure 2.8(c) and threshold distribution in Figure 2.8(d). Majority of the stations within this zone contain slopes from -0.1 to 0.1 [number of extremes/year]. The regions comprising this zone show different seasonal patterns. The Csa and Csb regions exhibit high

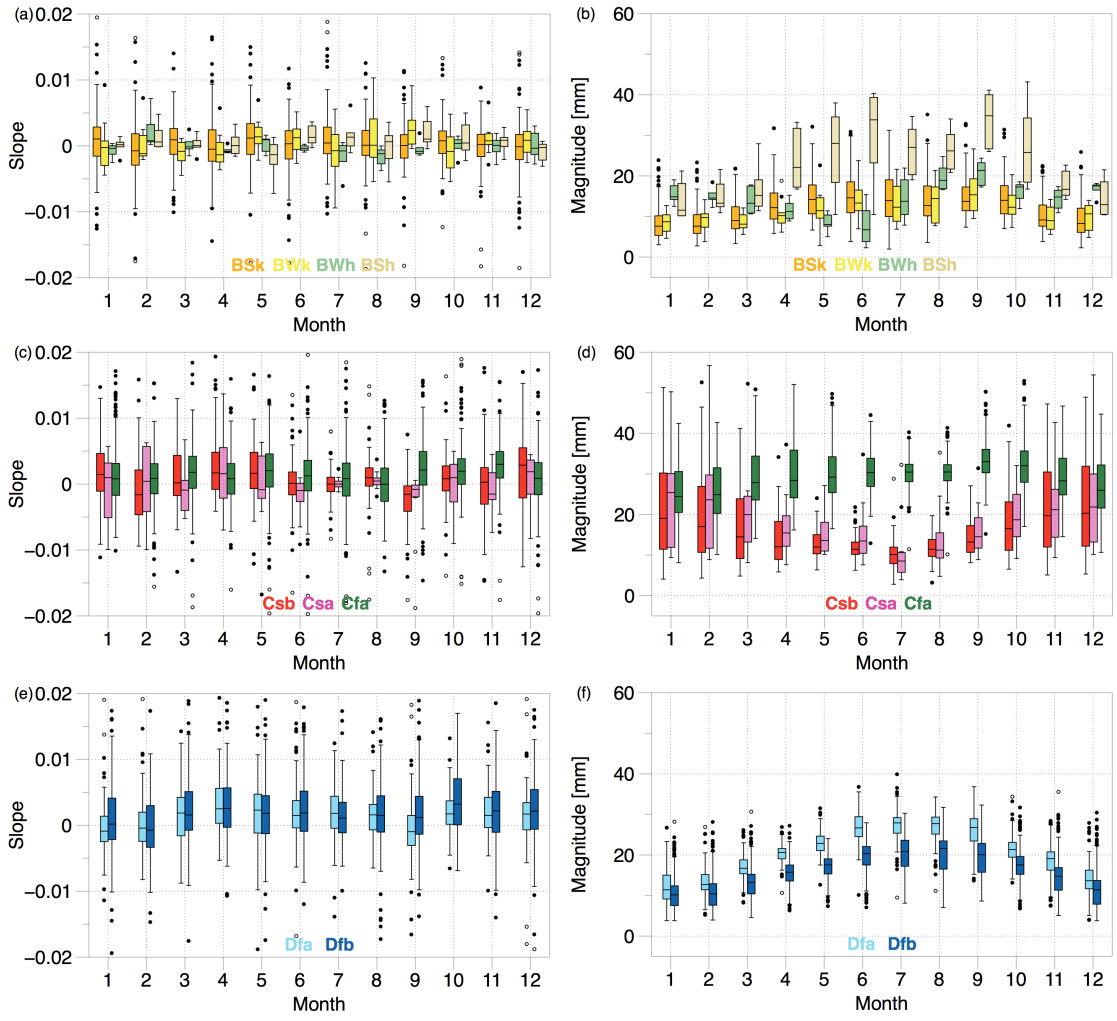

Figure 2.8 Mean slope [number of extremes/years of record] and magnitude [mm] values for extreme precipitation, calculated at all 921 stations. a) Slope values for Koeppen-Geiger B regions , b) Magnitude thresholds for Koeppen-Geiger B regions, c) Slope values for Koeppen-Geiger C regions, d) Magnitude thresholds for Koeppen-Geiger C regions, e) Slope values for Koeppen-Geiger D regions and f) Magnitude thresholds for Koeppen-Geiger D regions.

thresholds during the winter and lower thresholds during the summer. The Cfa region is largely of opposite phase, which is a more consistent and high threshold level.

The **snow zone** slope distribution is found in Figure 2.8(e) and threshold distribution in Figure 2.8(f). The snow zone contains roughly the same spread as the warm temperate zone, but with a slightly different range. The majority of the data fall into the -0.1 to 0.15 [number of extremes/year], which signifies greater precipitation extremes.

Extreme Maximum Temperature

The **arid zone** slope distribution is found in Figure 2.9(a) and threshold distribution in Figure 2.9(b). The slope values for all stations in this region have a range of -0.05 to 0.075 [number of extremes/year], majority of the means are above zero showing a skew to the positive trends versus negative. The magnitude thresholds show strong seasonality in maximum temperature extremes with a peak in July.

The **warm temperate zone** slope distribution is found in Figure 2.9(c) and threshold distribution in Figure 2.9(d). Slope values for this region exhibit a seasonal component. The majority of values lie within -0.05 to 0.05 [number of extremes/year]. The mean values tend to be positive for the winter months and negative for the summer months, meaning that overall this region is illustrating a gain in heat events in the winter and a loss of heat events in the summer. In terms of magnitude the typical seasonality associated with this climate is present.

The **snow zone** slope distribution is found in Figure 2.9(e) and threshold distribution in Figure 2.9(f). The range for this region lies within -0.025 and 0.05 [number of extremes/year]. A similar seasonal trend seen in the warm temperate zone can also be seen here in terms of the sign of the slope based on season. For the summer months the slope values increase in range as well as become negative. Where; win-

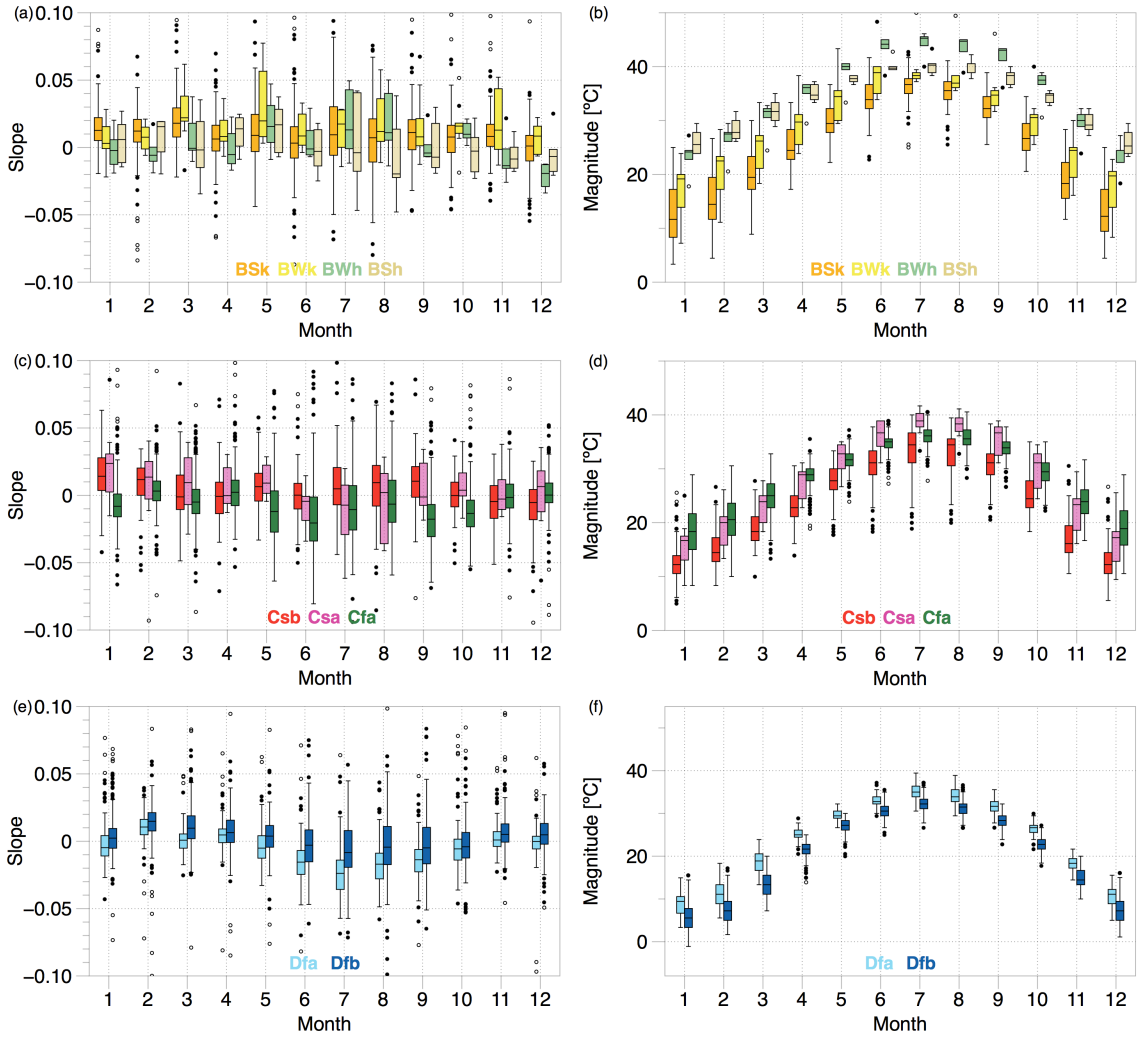

Figure 2.9 Mean slope [number of extremes/years of record] and magnitude [°C] values for extreme maximum temperature, calculated at all 921 stations. a) Slope values for Koeppen-Geiger B regions , b) Magnitude thresholds for Koeppen-Geiger B regions, c) Slope values for Koeppen-Geiger C regions, d) Magnitude thresholds for Koeppen-Geiger C regions, e) Slope values for Koeppen-Geiger D regions and f) Magnitude thresholds for Koeppen-Geiger D regions.

ter the ranges decrease and hover slightly above zero. The magnitude thresholds for extreme temperature in the snow zone follow normal seasonal cycle.

Extreme Minimum Temperature

The **arid zone** slope distribution is found in Figure 2.10(a) and threshold distribution in Figure 2.10(b). For this zone all regions exhibit a similar spread in slope value and all lie between -0.01 and 0.02 [number of extremes/year]. The mean slope values are all above zero and are indicative of positive mean values. In terms of seasonality within the magnitude, the BWh and BSh regions are closely related as well as the BWk and BSk regions. All regions follow a seasonal cycle of minimum temperature.

The **warm temperate zone** slope distribution is found in Figure 2.10(c) and threshold distribution in Figure 2.10(d). The Cfa region contains a smaller range and closer to zero mean and overall lies within -0.01 to 0.01 [number of extremes/year]. The Csa and Csb regions have a larger spread and larger range for this region. The slope values lie within -0.01 to 0.02 [number of extremes/year]. The magnitude thresholds results show a separation of eastern warm temperate from western warm temperate as well. The Cfa (eastern) region has a larger variation seasonally and is still around the same range with the Csa and Csb regions.

The **snow zone** slope distribution is found in Figure 2.10(e) and threshold distribution in Figure 2.10(f). This region has a small spread of slope values with a range from -0.01 to 0.01 [number of extremes/year]. The magnitude values are normal and vary by season for this region. Compared to the other zones the snow zones exhibit negligible long-term trend in minimum temperature extremes.

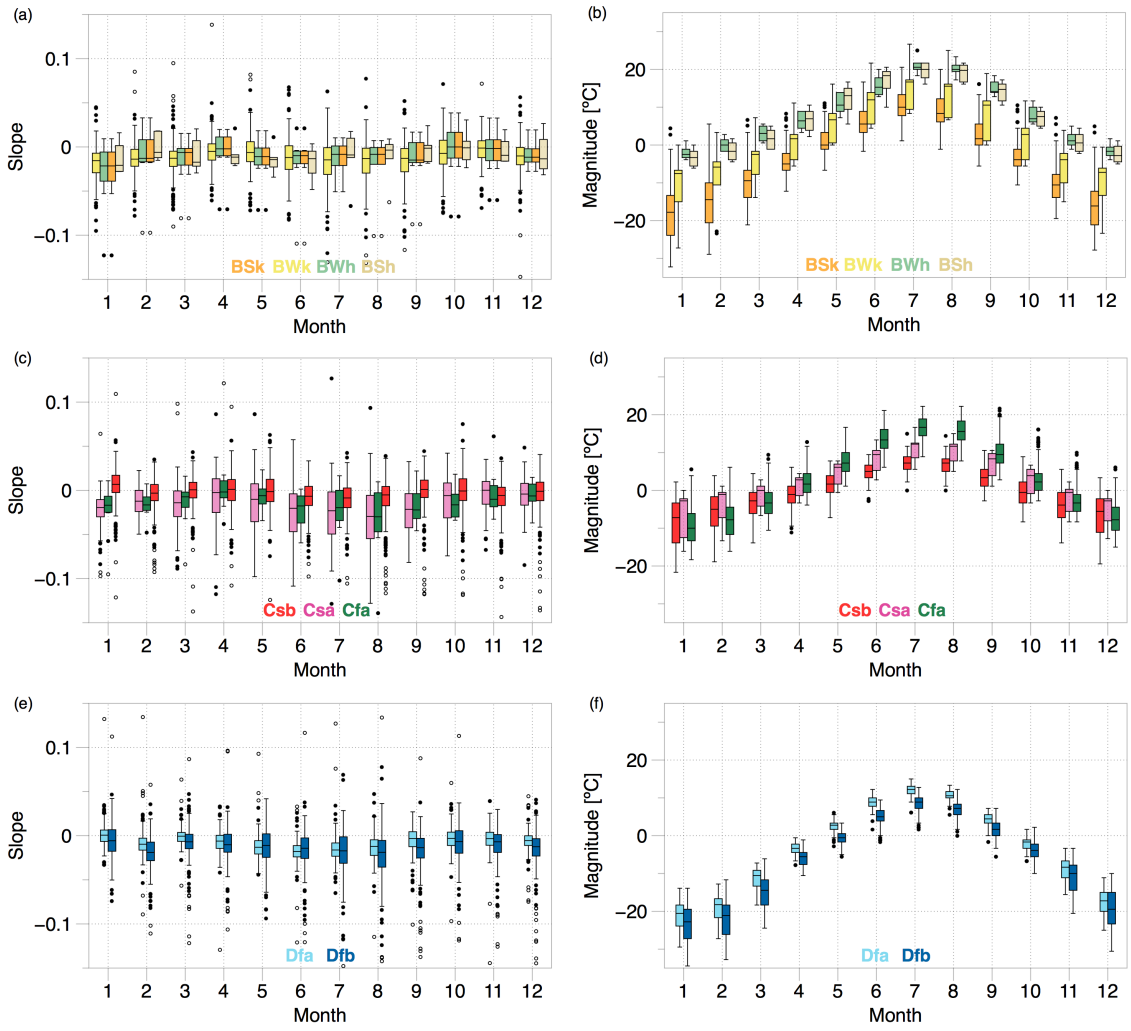

Figure 2.10 Mean slope [number of extremes/years of record] and magnitude (°C) values for extreme minimum temperature, calculated at all 921 stations. a) Slope values for Koeppen-Geiger B regions , b) Magnitude thresholds for Koeppen-Geiger B regions, c) Slope values for Koeppen-Geiger C regions, d) Magnitude thresholds for Koeppen-Geiger C regions, e) Slope values for Koeppen-Geiger D regions and f) Magnitude thresholds for Koeppen-Geiger D regions.

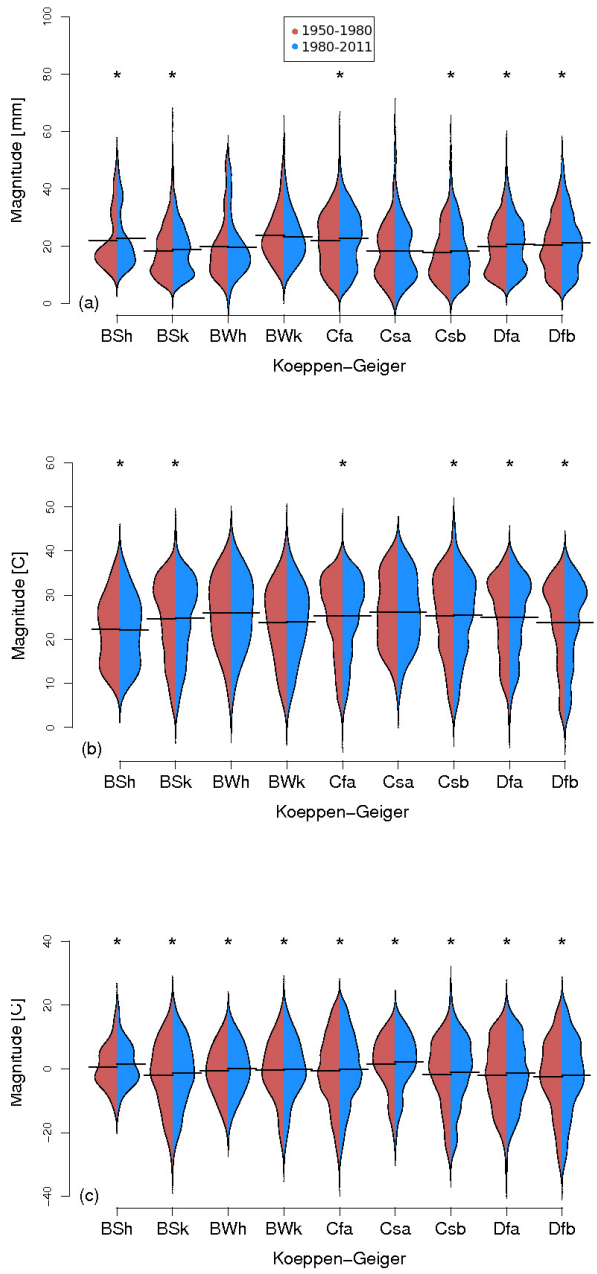

Figure 2.11 Two-sided bean plots comparing 1950-1980 and 1980-2011 monthly extreme magnitude thresholds. All 921 stations are represented and separated by Koeppen-Geiger region. (a) Extreme precipitation threshold [mm], (b) Extreme maximum temperature threshold (°C), (c) Extreme minimum temperature threshold (°C). The asterisk (*) indicates that there is a statistical difference between the two sampled groups, significant at the 95th percentile.

2.4.6 Recent Changes in Extreme Thresholds

The change in threshold for an extreme weather event to occur is assessed by comparing the data from 1950-1980 versus 1980-2011. The magnitude threshold for the 90th percentile is compared between each time series in Figure 2.11. A paired t-test was performed on the data with the null hypothesis being there is no difference between the two samples. The samples that reject the null hypothesis with 95% confidence are indicated by an asterisk. For extreme precipitation, the climate groups that are non-stationary are BWh, BWk and Csa. For extreme maximum temperature BWh, BWk and Csa are also non-stationary. All regions within extreme minimum temperature are non-stationary, the distribution of cold extremes is changing. The non-stationary results are indicative of a shifting climate, resulting in a new distribution of extreme events for the future. The large slope values indicate that most of the US has lost up to 20 cold events in the last century. The results show the nature of cold extremes are shifting, this is indicative of a warming climate.

2.5 Discussion

Extreme weather trends over the US exist and vary by Koeppen-Geiger Classification. Changes in the number of extreme precipitation events occur on the order of a magnitude smaller than of extreme temperature events. The northeast half of the country (regions Dfa, Dfb and Cfa) exhibit the greatest change in number of extremes in precipitation. Extreme maximum temperate events are decreasing by about 20 events (per 100 years) in the last century within the eastern US, and increasing by around 20 events (per 100 years) over the western states. Results show a reduction in the number of cold events in the last 100 years. This trend of a reduction on extreme temperature is present across all seasons and throughout all climate zones, except

over the southeast. With the projected increase of overall global temperature these extremes will only continue to vary. The greatest increase in extreme precipitation events in the past 100 years also exhibit the largest magnitude thresholds; therefore, the strongest rainfall events will become even stronger in the future. Extreme heat events tend to occur at temperatures above $30 - 35\,^{\circ}\mathrm{C}$ but can be as low as $15\,^{\circ}\mathrm{C}$ in the cold seasons. The extreme cold events along the coast, and eastern US occur under a higher threshold for an event to occur.

BSk (Rocky Mountains), BSh (Desert Southwest), Cfa (Southeast), Csb (West Coast), Dfa (Northern Midwest) and Dfb (North) are all non-stationary for extreme precipitation events. This result explains that the distribution of events is shifting. In each of these climate regions the mean has increased. In the new distribution, the threshold has increased in order for an event to be considered extreme, meaning what is considered an extreme precipitation event is changing. Extreme precipitation events in those climate regions are becoming more intense. For extreme maximum temperature the shift is occurring in the same regions, BSk, BSh, Cfa, Csb, Dfa and Dfb. For extreme minimum temperature the shift is occurring in every region across the US. Extreme cold days are now shifting to a warmer mean in order to be considered extreme. The extremes that existed 100 years ago are now shifting, and with the projected warming, will continue to shift.

Trends in temperature extreme indices computed from nine AOGCMs for the US have been in agreement with observations for the latter part of the 20th century. The trends indicate decreases in frost days, increases in growing season length, and increases in warm nights (Meehl et al., 2009). Models have been helpful in projections of future extreme events but, GCMs cannot accurately attribute the forcing mechanisms behind weather extremes (Easterling et al., 2000). Blekinsop et al (Blekinsop et al., 2008) have shown forcing mechanisms such as regional circulation patterns

have been known to impact the climate, and may also impact the nature of extreme weather events. Work has progressed on modeling extreme precipitation events and it has been found that NARCCAP models reproduce well several features (Gutowski et al., 2010).

Extreme events have been found to influence an increase of non-native species and decrease the biotic resistance of native communities (Diez et al., 2012). The Koeppen-Geiger analysis allows for understanding what native communities will be affected the most and allows for the development of mitigation strategies to prevent the profile ration of invasive species. More frequent extremes have led to other ecological and economic impacts. Frost formation, plant death and damage to sensitive plants have been witnessed (Stenseth, 2002). With the increase in global temperature and sensitivity to extremes, the agricultural industry has been impacted as well. An increase in growing season temperature has begun to stress crops and livestock at a global scale (Battisti and Naylor, 2009).

2.6 Conclusion

Recently the IPCC has put a strong emphasis on the impact of climate change on extreme weather events in regard to global climate change. A warming world has the ability to cause changes in extreme weather and climate events, which have the potential to result in unprecedented global climate extremes (IPCCSREX, 2012), (IPCC, 2007). Previous research has focused predominantly on global ramifications; this study explores the regional variability in the evolution of extreme statistics over the US. Understanding the spatial nature of changes in extreme events in the US can help lead to a better understanding of future alterations caused by climate change.

Changes in extreme weather events due to anthropogenic climate change may have

large impacts on local weather and climate. The knowledge gained from this study on extreme weather has provided insight into changes over the past century. The USHCN observations of daily precipitation and temperature values were used to evaluate the change in frequency and magnitude of extreme weather events from 1900-2011. These changes were categorized into nine regions defined by the Koeppen-Geiger climate classification system. Precipitation extremes were found to be decreasing in the fall and winter, increasing in the spring, with relatively little change in the summer. Maximum temperature extremes prove to be consistent or decreasing in the cooler months and increasing in the warmer months. Minimum temperature shows a trend indicative of a loss of extreme daily cold events except for the southeast. Regional analysis shows substantial spatial variability in the behavior of climate extremes in mean trends for all variables and extremes differ as a function of climate.

Chapter 3

The Impact of Teleconnection Patterns on the Spatial and Temporal Scale Dynamics of US Extreme Weather

3.1 Introduction

Climate is influenced by many factors and one area of climate variability that has received significant recent attention is the change in the pattern of extreme events. Heavy precipitation, severe heat and cold events, and changes in daily temperature ranges have become more frequent on a global scale (IPCC, 2007). Natural and anthropogenic contributions will both cause significant changes in a warming world, and the ability to isolate one source from another can often be difficult (IPCC, 2001). Natural variability includes and is not limited to changes in, solar radiation, atmospheric and surface properties, energy partitioning and large scale circulation patterns. An-

thropogenic contributions include any human alteration to a natural process. One way to gain understanding of climate change is to focus on understanding the reaction to forcings from the past.

Blekinsop et al. (2008) have shown that forcing mechanisms such as regional circulation patterns impact the climate, and may also impact the nature of extreme weather events. Regional circulations are often impacted by teleconnection patterns such as El Niño/Southern Oscillation (ENSO), Pacific Decadal Oscillation (PDO), North Atlantic Oscillation (NAO), and the Atlantic Multidecadal Oscillation (AMO). Since midlatitude climate extremes have been shown to be associated with these low-frequency teleconnection patterns (Blekinsop et al., 2008), it is important to understand this as a possible forcing mechanism and assess the temporal variation they may cause on weather extremes. One teleconnection in particular, PDO, has been shown to influence the precipitation patterns of the west coast of the US (Mantua et al., 1997) as well as the desert southwest (Meehl et al., 2010), specifically, summer precipitation extremes in the western US are most influenced by PDO (Nigam et al., 1999). Higher frequency teleconnection patterns, such as ENSO, tend to have similar influences on the regional circulation patterns. During strong ENSO signals, the US is impacted by either drier and warmer conditions or cooler and wetter conditions. These climate impacts depend on the ENSO signal, a negative value signifying an El Niño signal (warm and dry) and a positive value signifying a La Niña signal (cool and wet) (Neelin et al., 1998). PDO follows similar ENSO-like patterns and can either intensify or weaken the ENSO signal to produce an even more extreme forcing on regional circulation patterns depending upon the coherence of the teleconnection and weather event. The warm phase of PDO corresponds with El Niño-like weather anomalies, similarly, the cool phase of PDO corresponds with La Niña-like climate patterns. Not only does the strength of the phase interact with regional circulation

patterns to produce extreme events, but the change between phases can also impact the weather and, in theory, extreme weather events.

Understanding the influence of regional teleconnections may enhance the ability to forecast extreme weather. In terms of extreme precipitation, ENSO based predictability is potentially high along the Gulf Coast, Central Plains, Southwest, Ohio River Valley and Florida (Gershunov and Barnett, 1998). ENSO has been known to increase the median precipitation beyond the 70th percentile for El Niño years and below the 30th percentile for La Niña years, indicating more precipitation (monthly total) during each phase (Smith and Ropelewski, 1997). Increased flooding is an important aspect of this hydrological response to ENSO and one effect is that steam flow is amplified over that of an extreme precipitation event (Cayan et al., 1999). Specifically four regions of the US appear to have a coherent ENSO response for extreme precipitation, the mid-atlantic, the high-plains, the great basin and the southwest (Ropelewski and Halpert, 1986). In the western US the largest fraction of extreme precipitation events occur during El Niño winters (Higgins et al., 2000). US precipitation is not only enhanced by ENSO, Barlow et al. (2001) found that there is a significant relationship between some primary nodes of pacific variance, specifically, PDO. ENSO teleconnections with precipitation are often weakly correlated with positive PDO (McCabe and Dettinger, 1999).

Global models have been used to simulate 21st century climate which induces low-frequency variability like El Niño Southern Oscillation (ENSO) events in aim to help understand dynamics under future climate change. These simulations show stronger precipitation for the southern states, accompanied by an increase in heat waves in correspondence with El Niño events (Meehl et al., 2007b). This explains that while precipitation is largely influenced by teleconnections there is also an influence on extreme temperature. Results from several earlier global climate model studies

indicate that as global temperature rises due to anthropogenic influences, the mean Pacific climate will tend to resemble an El Niño state more frequently (Knutson and Manabe, 1995; Latif et al., 1999; Meehl and Washington, 1996). Wolter et al. (1999) have confirmed that El Niño-like conditions create very warm winters for the Pacific Northwest and very cold winters along the Gulf coast. In recent years scientists have increasingly invoked ENSO as a cause for a broad array of climate extremes. Overall, extreme short term climate anomalies (extreme events) have enormous consequences for the US (Hughes, 1982; Riebsame et al., 1991; Trenberth, 2009).

To understand the covariability of teleconnections and extreme weather, a technique that can isolate influences across different time scales is required. One method is the use of wavelet decomposition. Wavelet analysis allows the variation between the geographical patterns of extreme events and low frequency teleconnection patterns to be quantified. The teleconnection patterns of interest here are ENSO, which has been shown to be broadband with a spectral intensity peak around 4 years (Kleeman, 2002), and Pacific Decadal Oscillation (PDO). Higgins et al. (2000) also found that there is a coherent relationship with the location of extreme precipitation and enhanced tropical convection on intra seasonal timescales. Changes in tropical convection can be caused by ENSO-like sea surface temperature swings which have been found to occur at various timescales ranging from inter annual to inter decadal (Weng et al., 1999; Zhang et al., 1997). This paper aims to understand the timescales at which extreme weather events occur, the role teleconnection patterns play and the associated geographical variability.

3.2 Data

Research was conducted with the use of The United States Historical Climate Network (USHCN) (Menne et al., 2011). The USHCN was developed by the National Oceanic and Atmospheric Administration (NOAA) National Climatic Data Center (NCDC) in order to better detect climate change. The weather data used for analysis was daily precipitation, maximum temperature and minimum temperature from 1900-2011. For optimal time series lengths, stations missing more than 10 years of data were eliminated, resulting in 958 of the total 1,218 USHCN towers used in this study.

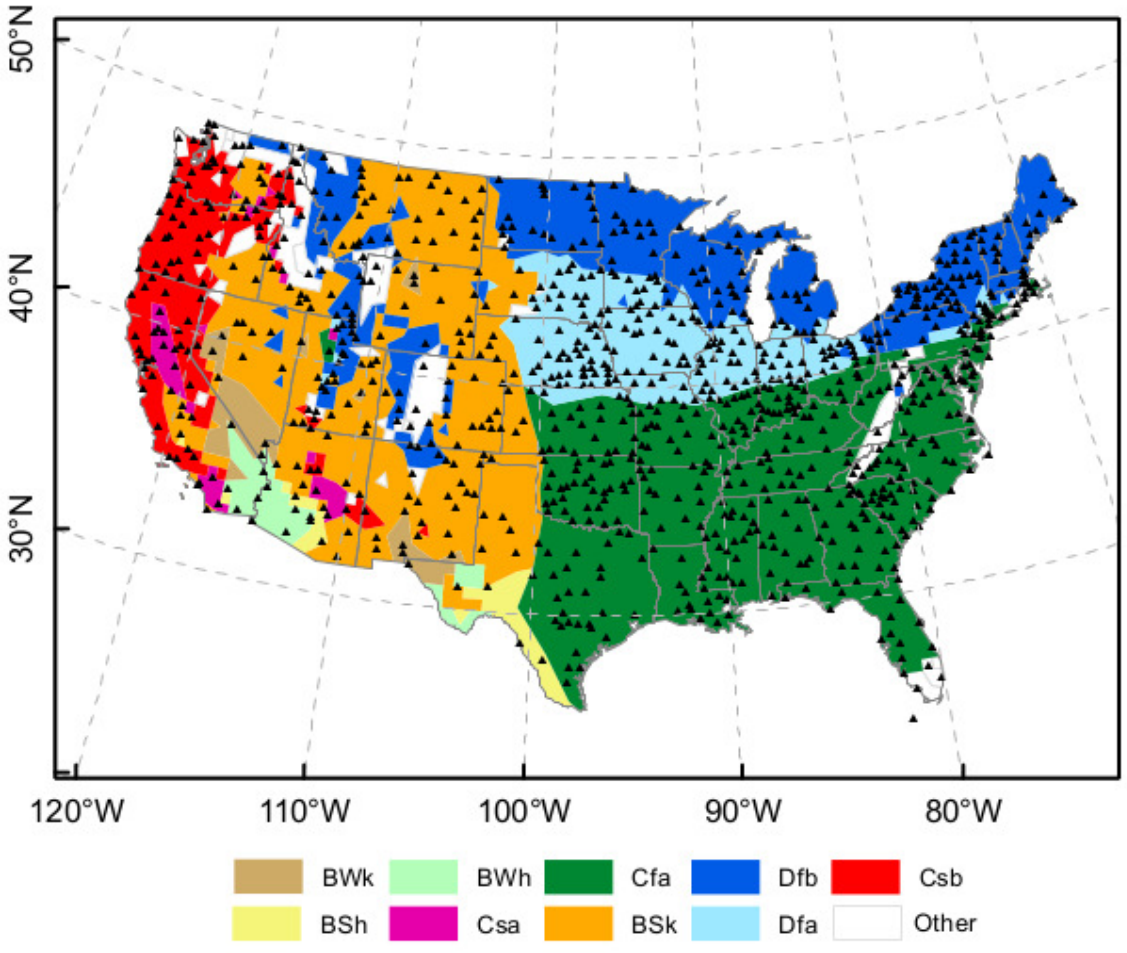

Figure 3.1 USHCN station distribution with corresponding Koeppen-Geiger classification.

KG Zone	KG Region	USHCN Count
Arid	BSh	6
	BSk	135
	BWh	6
	BWk	10
		Total: 157
Warm Temperate	Cfa	337
	Csa	13
	Csb	83
		Total: 443
Snow	Dfa	148
	Dfb	183
		Total: 331
Other		**Total: 37**

Table 3.1 Distribution breakdown for KG zone, KG region and USHCN stations. The main classification zones are: B-arid, C-warm temperature and D-snow. The precipitation classification groups are: W-desert, S-steppe, f-fairly humid and s-summer dry. The temperature classification groups are: h-hot arid, k-cold arid, a-hot summer and b-warm summer. The selected climate regions represent 95% of the area within the US are: BSh, BSk, BWh, BWk, Cfa, Csa, Csb, Dfa and Dfb. All other regions are listed as other.

In order to understand the variability as a function of geographic space, a climate classification system is used. The most common way to classify climate is using the Koeppen-Geiger (KG) classification system (Kottek et al., 2006). Utilizing the KG system provides insight into the relationship between regional extremes and teleconnection patterns. Since 95% of the US lies in 9 climate zones, which focuses the analysis on those specific regions. These 9 groups cover a wide range of climate classes and a breakdown can be found in Table 3.1. Figure 3.1 shows the USHCN station distribution as well as the KG classification.

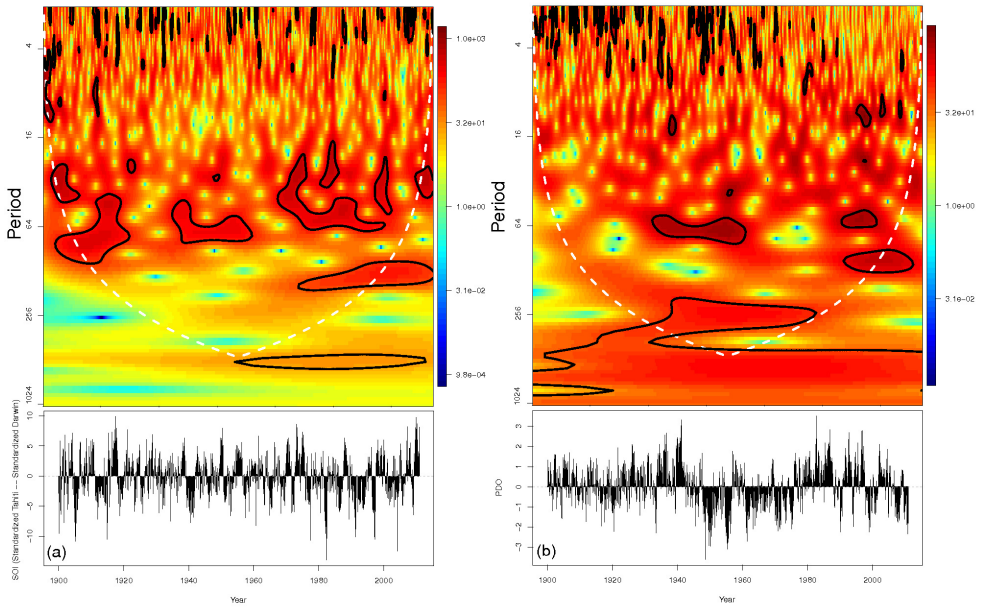

Figure 3.2 Continuous wavelet transform (*cwt*) results for the teleconnection patterns. Southern Oscillation Index where the standardized values are based on Trenberth (1984) (a). Pacific Decadal Oscillation Index where the standardized values are based on Mantua et al. (1997) and Zhang et al. (1997) (b).

Since teleconnections play a major role in regional climate extremes, this study investigated the role of ENSO and PDO on US daily weather. There are many ENSO indices and the Southern Oscillation Index (SOI) was chosen to represent ENSO because it combines the Southern Oscillation into one series and has a long enough

record to match the dataset. The SOI index used in this study was computed using monthly mean sea level pressure anomalies at Tahiti and Darwin and processed by The National Center for Atmospheric Research (NCAR) (Trenberth, 1984). The PDO data used in this study originates from the United Kingdom Meteorological Office (UKMO) historical dataset and is processed by the University of Washington (Mantua et al., 1997). Both SOI and PDO signals are shown in Figure 3.2.

3.3 Methodology

3.3.1 Wavelet Analysis and Significance

For this study, an extreme event is quantified as an event that occurs above the 90th percentile of its monthly bin. There is a monthly bin for each month and the total number of months in each bin is based on the length of record. The monthly threshold values were calculated based on Wilson et al. (2013) and are found to be unique for each station. This methodology provides a date for each extreme weather event and can be used for assessing normal weather events against those of extreme responses.

Geophysical time series can often exhibit non-stationarity, contain dominant periodic signals and hidden patterns. These time series can be decomposed using wavelets into signals, that vary in both time and frequency space. Long-term weather data can exhibit this periodic behavior as well as long-term climate patterns such as ENSO and PDO. Wavelet analysis allows the weather time series and the teleconnection signals to be analyzed at different periods throughout the length of the signal. They also provide the ability to simultaneously view the spatial and temporal nature of an extreme weather event against those of a normal weather event. For this study all wavelet transforms (continuous wavelet transform (cwt), wavelet cross wavelet transform (xwt) and wavelet transform coherence (wtc)) were conducted using the

Biwavelet package (Gouhier and Grinsted, 2013) in R. Wavelet transform is chosen over Fourier transform due to the frequency localization limitation with Fourier transforms. Wavelets analysis avoids this issue by simultaneously decomposing in time space and frequency space. This allows for information regarding the power of any periodic signal as well as how that power varies over time.

The wavelet transform is conducted by translating (n) and dilating (m) the mother wavelet (ψ) across the time series (X) as a function of time ($f(t)$):

$$W_f^X(m,n) = \frac{1}{\sqrt{n}} \int_{-\infty}^{\infty} f(t) \bar{\psi} \frac{t-m}{n} dt \tag{3.1}$$

where the initial time scale is 2^1 (2 days) and the mother function, selected as a Morlet wavelet, is given by:

$$\psi_0(x) = \pi^{-\frac{1}{4}} e^{iw_0\eta} e^{-\eta^2/2} \tag{3.2}$$

where w_0 is the frequency. For this study the main results will be in terms of the wavelet power spectra, the choice of the mother wavelet function is not critical, and one function will give the same qualitative results as another (Torrence, 1998). Since the Morlet wavelet is complex, contains many oscillations, combines both positive and negative peaks into a single broad peak (Torrence, 1998) and is commonly used it will satisfy the needs of this paper. With this given wavelet function, the necessary scales/periods chosen will be reflective of the length of the time series. Since Morlet is non-orthogonal, it is not limited to a discrete number of scales, and an arbitrary set of scales can be used to build the spectra. It is common to see scales/periods written as fractional powers of 2 (Torrence, 1998). The *cwt* calculations focused on the timescales 2^1 - 2^{13} in order to capture the daily to decadal responses. This corresponds to variability from 2 to 8192 days (approximately 20 year cycles). Though the time series for some stations can handle longer periods (2^{14} which equates to 16304 days) this scale was the longest consistent period for all 928 stations used. The *xwt* and

wtc used the same timescale but timescales less than 30 days were removed from the *xwt* and *wtc* calculations due to the fact the SOI and PDO time series are calculated as monthly mean values. Decomposition from monthly to multidecadal is sufficient in understanding the possible influence of low-frequency oscillations on extreme weather events, since SOI is a roughly 3-5 years in cycle and PDO cycles between 50-70 years.

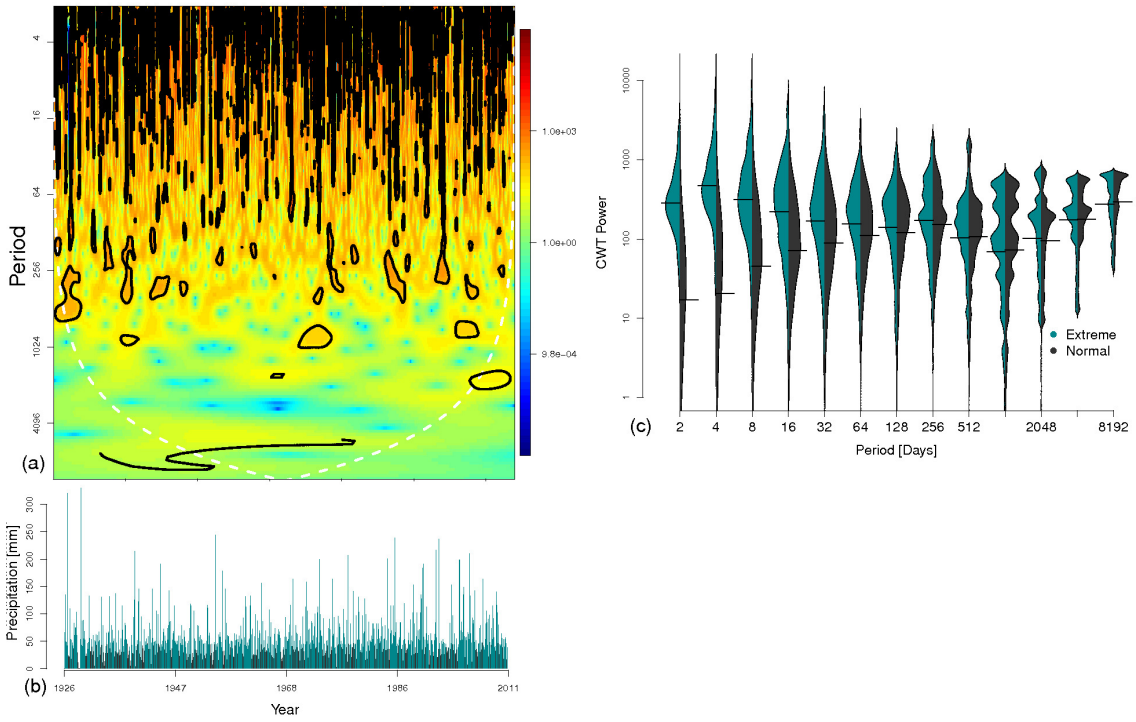

Figure 3.3 Results for Brewton, AL (USHCN Station 011084) daily precipitation continuous wavelet transform (*cwt*) (a), precipitation time series with extreme event highlighted (b) and bean plots representing the pdf of extreme or normal events at each timescale (c).

The *cwt*'s were conducted on the precipitation, maximum temperature and minimum temperature time series for each USHCN station as well as the SOI and PDO time series. In order to determine the dominant mode of variability for extreme weather, the normal and extreme days were then selected out of each *cwt* response. To gage the response as a function of climate zone each *cwt* was then averaged across

their specific Koeppen-Geiger (KG) region. This process is similar to what Torrence (1998) explained as *averaging in time*, where a slice through the scale of the wavelet plot is taken as a measure of the local response. These localized responses are taken separately for each extreme day and normal day and then averaged across each period to provide a final solution for a single localized response over time. An example of this process is shown for Station Number 011084 (Brewton, Al) in Figure 3.3 (a), where 3.3a shows the wavelet transform, 3.3b illustrated the time series highlighting the extremes and 3.3c provides detailed information about each probability density function (pdf) for the extreme and normal series and the average response for each scale. This process was completed for each station and then averaged across the 9 KG regions.

In order to understand the relative influence of teleconnection patterns on extreme weather, the cross wavelet transform (xwt) and wavelet transform coherency (wtc) were calculated. The xwt transforms are indicative of the local relative phase connection, while wtc is simply an analysis of the coherency between the two data sets at a range of scales and through time.

Given two time series X and Y, the cwt for each can be defined as $W_f^X(m,n)$ and $W_f^Y(m,n)$, thus the cross-wavelet is denoted as $W_f^{XY}(m,n)$. Since the cross wavelet is complex, the cross wavelet power is then $\left|W_f^{XY}(m,n)\right|$. The theoretical distribution of the xwt of two time series with background power spectra P_k^X and P_k^Y is given in Torrence (1998) as:

$$D\left(\frac{\left|W_f^{XY}(m,n)\right|}{\sigma_X * \sigma_Y} < p\right) = \frac{Z_\nu(p)}{\nu}\sqrt{P_k^X P_k^Y} \tag{3.3}$$

where $Z_v(p)$ is the confidence level associated with the probability p for a pdf defined by the square root to the product of two χ^2 distributions (Grinsted et al., 2004). σ is the standard deviation for each distribution, P_k is the assumed background power

spectra (ie. white or red noise). ν is equal to 1 for real and 2 for complex values.

Grinsted et al. (2004) have shown that the cross wavelet power reveals areas with high common power, and it is also useful to distinguish how coherent the cross wavelet transform is in time frequency space. Following Torrence and Webster (1998) the *wtc* is defined as:

$$R_f^2(m,n)) = \frac{S(s^{-1}\left|W_f^{XY}(m,n)\right|^2)}{S(s^{-1}\left|W_f^{X}(m,n)\right|^2) * S(s^{-1}\left|W_f^{Y}(m,n)\right|^2)} \tag{3.4}$$

where S is a smoothing operator, defined as:

$$S(W) = S_{scale}(S_{time}(W_f(m,n))) \tag{3.5}$$

where S_{scale} denotes smoothing along the wavelet scale axis and S_{time} smoothing in time (Grinsted et al., 2004) and s is defined as the circular standard deviation:

$$s = \sqrt{-2ln(R/n)} \tag{3.6}$$

where $R = \sqrt{X^2 + Y^2}$. The circular standard deviation is analogous to the linear standard deviation in that is varies from zero to infinity.

To ascertain the change in the relative influence of SOI and PDO signals on the extreme events to the normal, the *xwt* and *wtc* power spectrums were calculated and averaged for extreme days and normal days across each climate zone (an example is found in Figure 3.4). The example plot shows the *xwt* and *wtc* results for the decompositions of precipitation and SOI in Brewton, Alabama. The *xwt* and *wtc* plots are shown with the precipitation time series and the SOI signal. The extreme against those of a normal signal is not shown but follows the same process for *averaging in time* and is shown in Figure 3.4. This process was also completed for each station and then averaged across the 9 KG regions the same as described above. Both *xwt* and *wtc* were calculated for precipitation, maximum temperature, minimum temperature, SOI and PDO timeseries.

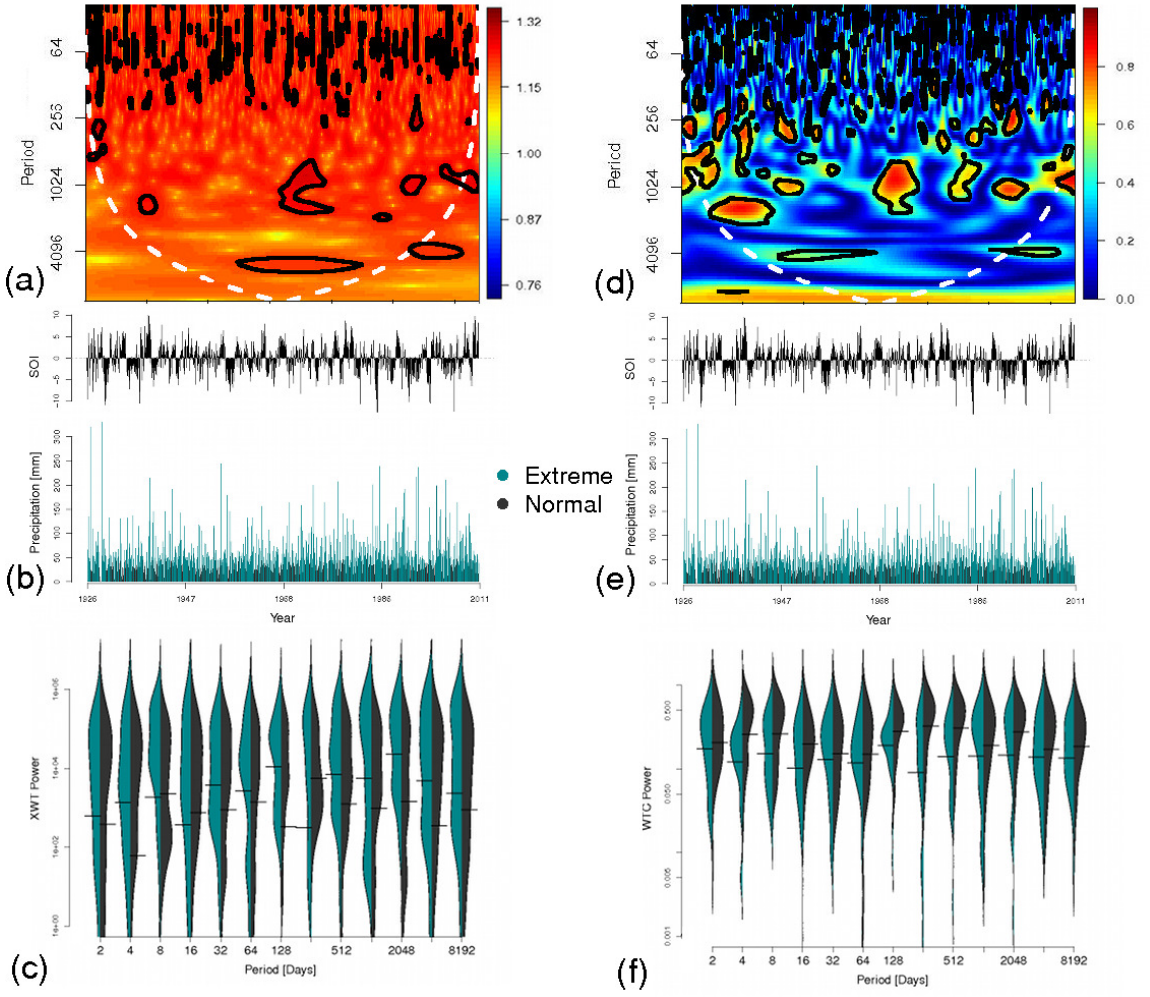

Figure 3.4 Results for Brewton, AL (USHCN Station 011084) daily precipitation and SOI behavior (a) cross wavelet transform (*xwt*), (b) the observed precipitation trend with the extremes highlighted alongside the observed SOI trend and (c) illustrating the power distribution of extreme and normal events for each period. The *wtc* example results are shown the the following column (d) the wavelet coherence transform, (e) the observed precipitation and SOI and (f) the power distribution of the extreme and normal events throughout time.

In order to determine if the response (*cwt*, *xwt* and *wtc*) for an extreme event is significantly different than a normal event, a paired t-test was used. The difference between each response at each time scale was considered significant when the p-value was ≤ 0.05, meaning that the extreme weather behaves differently then the normal weather signal.

The following nomenclature will be used in this paper; precipitation against those of a SOI (ppt, soi), precipitation against those of a PDO (ppt, pdo), maximum temperature against those of a SOI $(tmax, soi)$, maximum temperature against those of a PDO $(tmax, pdo)$, minimum temperature against those of a SOI $(tmin, soi)$ and minimum temperature against those of a PDO $(tmin, pdo)$.

3.4 Results

3.4.1 Overview

Prior to examining the response of extreme events to low frequency teleconnections, results will be discussed by decomposition type (*cwt*, *xwt* and *wtc*) and within those main groups further discussed by KG response (Arid, Warm Temperate and Snow Zones (Table 3.1)).

3.4.2 Scales of variability governing extreme events (*cwt* response)

The average *cwt* decomposition for extreme and normal events within each KG zone are shown in Figure 3.5. Precipitation is column 1 (3.5a, 3.5b and 3.5c), maximum temperature is column 2 (3.5d, 3.5e and 3.5f) and minimum temperature is the last column (3.5g, 3.5h and 3.5i). The extreme spectra are shown as a dashed line where

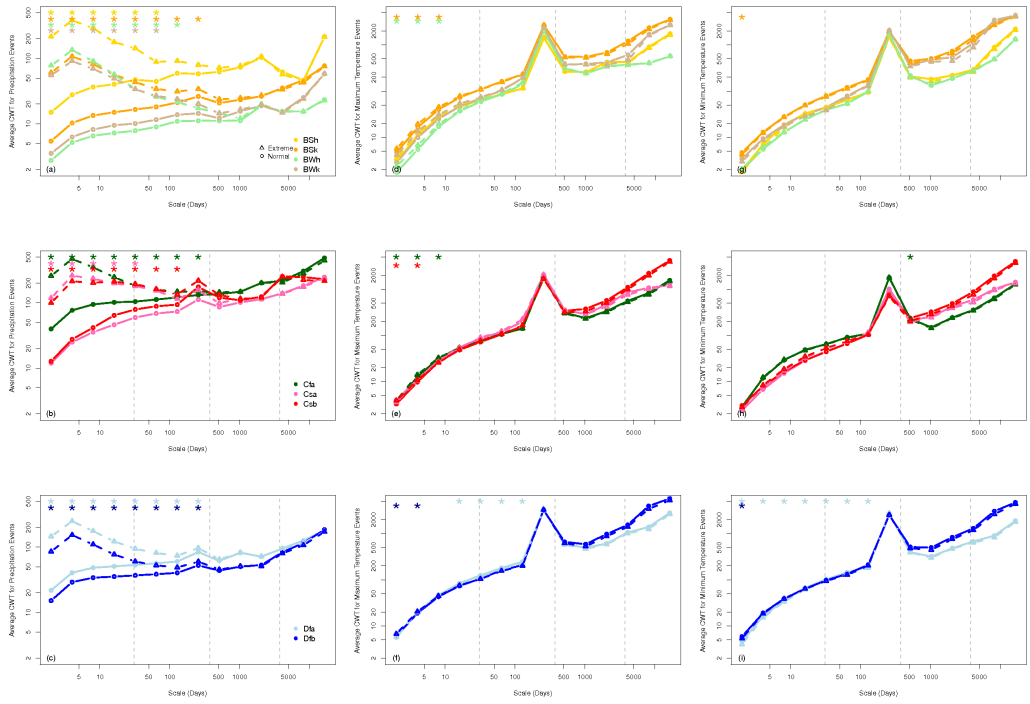

Figure 3.5 Continuous wavelet transform (*cwt*) results for precipitation (a-c), maximum temperature (d-f) and minimum temperature (g-i). Extreme (dashed) and normal (solid) results averaged across each Koeppen-Geiger region, where the arid zone is row 1, warm temperate zone is row 2 and snow zone is row 3. Vertical dashed grey lines are indicative of monthly, annual and decadal timescales respectively.

the normal spectra is a solid line. Scales that show a significant difference between the extreme and normal are shown with an asterisk and are significant at a p-value ≤ 0.05. Each time series was decomposed using a *cwt* at each USHCN station, and then averaged across 9 KG regions and grouped into 3 zones (Arid, Warm Temperate and Snow) the number of stations in each climate zone is shown in Table 3.1.

Precipitation

Precipitation extremes are significantly different from normal events at many scales. In the arid zone extreme precipitation differs from normal precipitation at periods of 4 through 64 days in all 4 regions (BSh, BSk, BWh and BWk). Extreme precipitation continues to exhibit a different response in BSk up to 128 days and BWh up to 256 days. In the warm temperate zone extreme precipitation shows a different pattern of significance within the period of 4-256 days for Cfa, 4-32 days for Csa and 4-128 days for Csb. For the snow zone both Dfa and Dfb spectras are significantly different at 4-256 days.

Maximum Temperature

Maximum temperature shows less scales with significant differences. This weather time series is significantly different between the two spectrass and are mainly focused on events below the monthly scale. For the arid zone, the extreme scales are significantly different at the 4-16 day period for all regions. For the warm temperate zone Cfa shows a difference at 4-16 day period, while Csa is 4-8 days, and there is no difference within Csb. The snow zone shows the most significantly different periods, with Dfa proving separation from 16-128 days and Dfb from 4-8 days.

Minimum Temperature

The *cwt* of extreme minimum temperature events does not vary much from the normal events. The arid zone shows one significantly different period at 4 days in BSh, the warm temperate zone shows no significantly different periods. The only region which shows a string of significantly different power spectras is the Dfa region within the snow zone at 4-256 days as well as a single period at 4 days for Dfb.

3.4.3 Assessment of phase connectivity (xwt response)

The xwt assesses the differences between the local relative phase connectivity. Each weather time series and SOI or PDO power specters are shown in Figures 3.6, 3.7 and 3.8 and have been averaged by extreme response and normal response across KG zone. In order to better understand the xwt relationship, where there is high common power, there is also a local relative phase connection between the two time series. That is, results with high power show phase togetherness where low power indicates out of phase results (Grinsted et al., 2004). For example, both ppt, pdo and ppt, soi become more in phase with each other throughout time, indicating that precipitation has a high power spectrum which is significant on longer timescale, indicative of ENSO and PDO.

Precipitation and Teleconnections

The influence of SOI and PDO on extreme weather is shown in Figure 3.6, column 1 (SOI) and column 2 (PDO). For SOI, all zones (arid, warm temperate and snow) exhibit many more significant differences between extremes and the normal response. PDO causes significant differences for all 9 regions between 32-256 days, except BSh, BWk and Csa which only show a significantly different response at a period of 32 days.

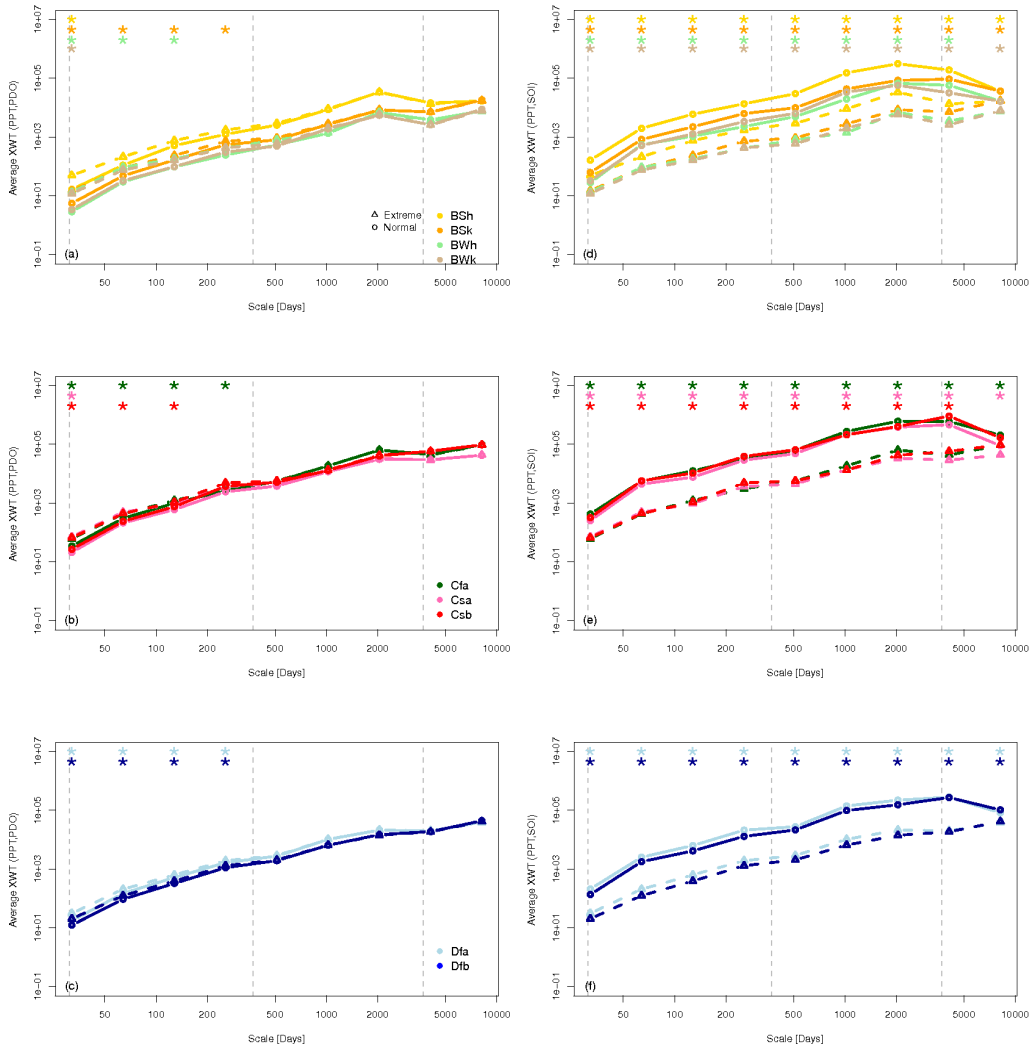

Figure 3.6 Cross wavelet transform (*xwt*) results of precipitation and teleconnections. Extreme (dashed) and normal (solid) results averaged across each Koeppen-Geiger region, where the arid zone is row 1, warm temperate zone is row 2 and snow zone is row 3. Vertical dashed grey lines are indicative of monthly, annual and decadal timescales respectively.

For SOI, all regions, except BWh and Csb, show significantly different responses for all scales, when looking at extreme events against those of a normal response. As expected the power increases in time, showing that there is a phases relationship at the longer timescales (where SOI and PDO oscillate).

Maximum Temperature and Teleconnections

The influence of SOI on maximum temperature is shown in Figure 3.7, where column 1 shows SOI and column 2 PDO. Unlike the precipitation response for xwt, the highest power is found roughly around the annual timescale, indicating phase connectivity between the two values is at the annual scale. There are less scales that are significantly different from extreme to normal than the precipitation results, and for maximum temperature they are much more scattered instead of in sequence throughout the scales.

For $xwt(tmax, pdo)$ there is no real pattern found with specific zones but mores variability across scale within regions. The arid zone indicates that BSh extremes are significantly different at periods of 32, 512 and 1024 days. BWh zone extremes are only different at the 32 time scale. For the warm temperate zone, the only regions indicating a different response for extremes are Cfa (32, 128 and 1024 days) and Csb (512 and 1024 days). The snow zone has the most periods with significant differences which are found in both Dfa and Dfb between 128-1024 days and 64-4096 days respectively.

For $xwt(tmax, soi)$ the same inconsistency throughout scales is found. For the arid zone the significantly different scales are found in BSk (1024-4096 days), and BWh (64 days). The warm temperate zone shows that Cfa (32, 1024 and 2048 days), and Csb (512-1024 days) have significantly different responses for extreme maximum temperature events. Again the snow zone contains the most significantly different

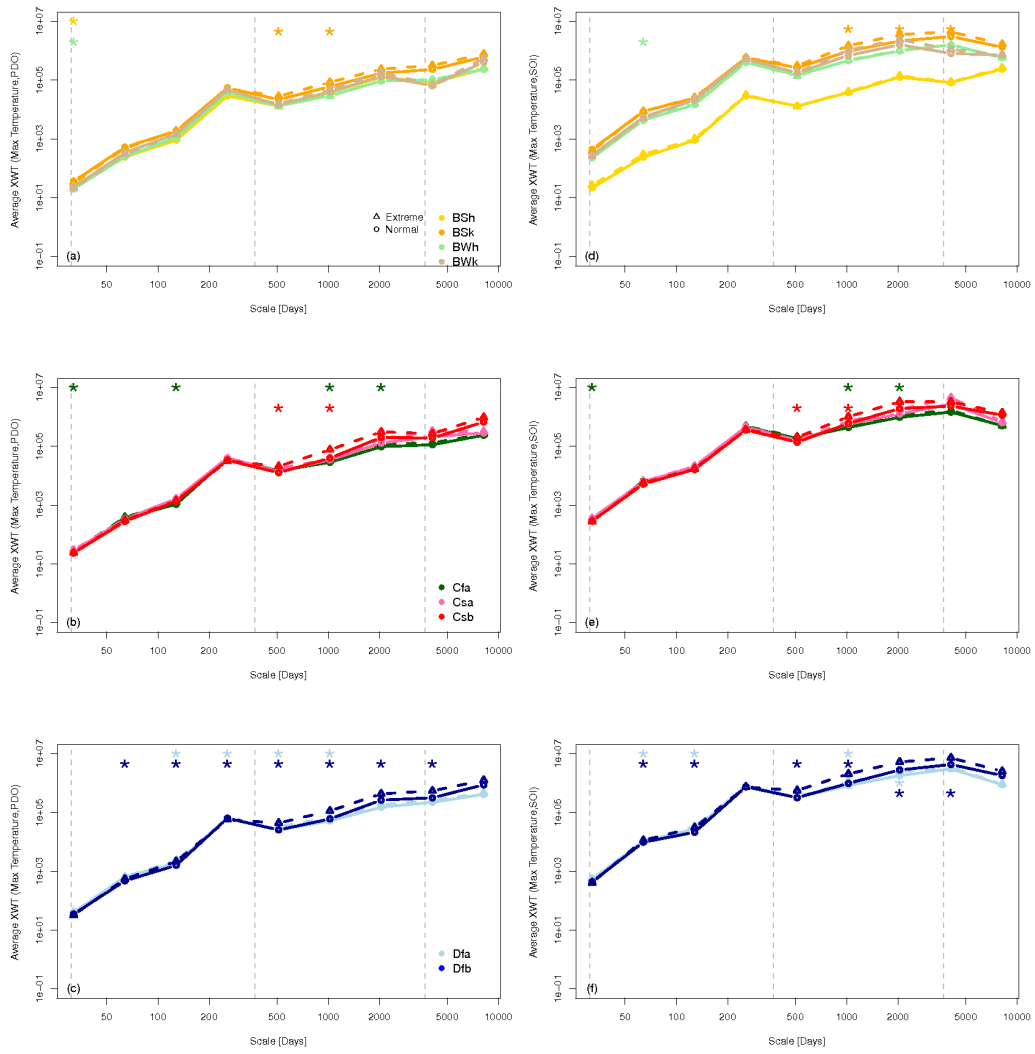

Figure 3.7 Cross wavelet transform (xwt) results of maximum temperature and teleconnections. Extreme (dashed) and normal (solid) results averaged across each Koeppen-Geiger region, where the arid zone is row 1, warm temperate zone is row 2 and snow zone is row 3. Vertical dashed grey lines are indicative of monthly, annual and decadal timescales respectively.

responses, Dfa at a period of 64 days, 128 days and 1024-2048 days, and Dfb with 64-4096 days.

Minimum Temperature and Teleconnections

The average arid, warm temperate and snow zone power spectra responses to teleconnections are shown in Figure 3.8, with column 1 being SOI and column 2 being PDO. Like maximum temperature, minimum temperature shows the largest phase connectivity at the annual timescale.

The arid zone shows different responses for $xwt(tmin, pdo)$ solely within BSk between periods of 32-128 days. The warm temperate zone has multiple regions with different power responses which are Cfa (32, 64, 256 and 1024 days) and Csb (32-64 days). The snow zone again has the most consistency (ie. most scales with significant differences in sequence) which indicates that within the Dfa and Dfb region there is a difference between extreme and normal power spectra at 32-256 days at 32-128 days, respectively.

The $xwt(tmin, soi)$ results show significance across scales for extremes having different power spectrass than a normal minimum temperature response. In the arid zone those regions are BSh and BSk at a period of 64 days, BSk between 32-128 days and BWk at 32, 64 and 256 days. In the warm temperature zone those regions are Cfa between 32-512 days, Csa at 32-64 days and Csb at 32-256 days. For the snow zone both Dfa and Dfb have the same significance within 32-512 days.

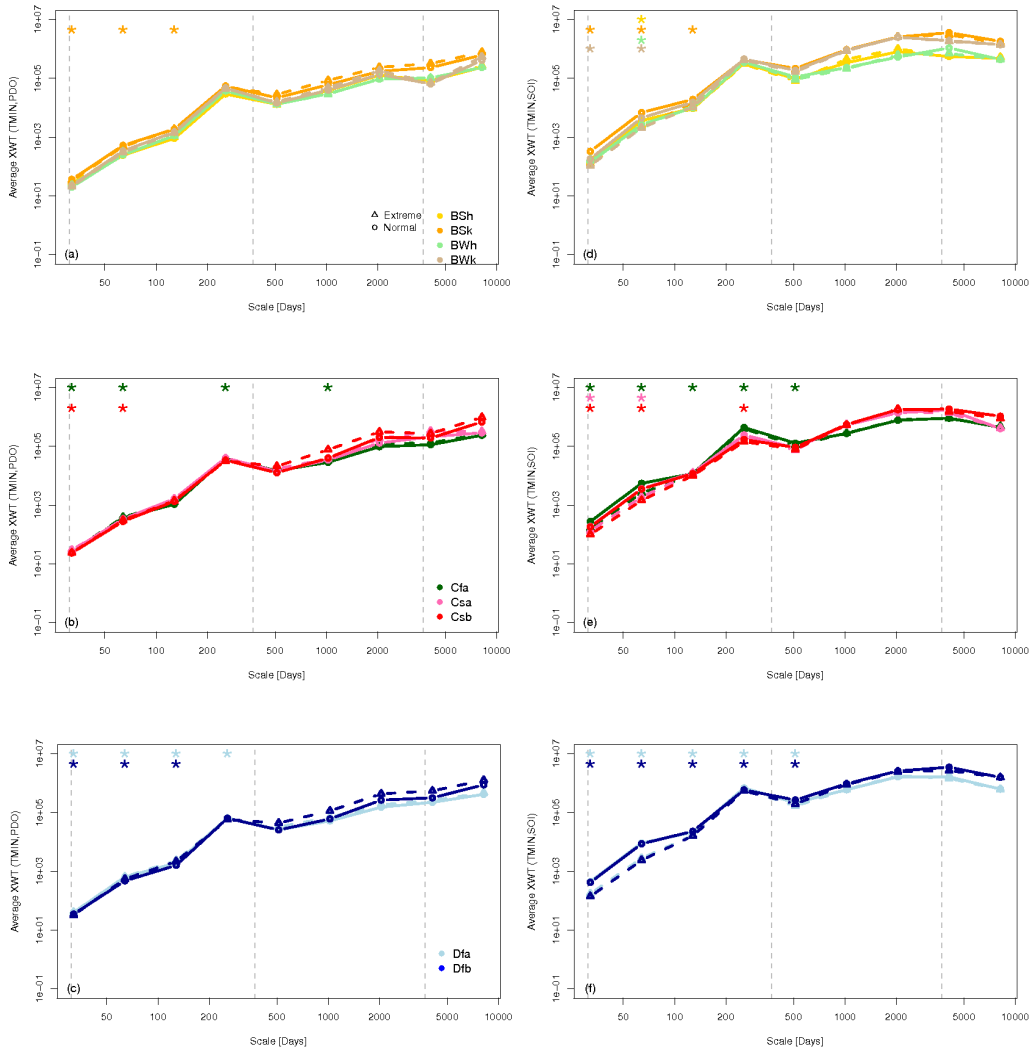

Figure 3.8 Cross wavelet transform (*xwt*) results of minimum temperature and teleconnections. Extreme (dashed) and normal (solid) results averaged across each Koeppen-Geiger region, where the arid zone is row 1, warm temperate zone is row 2 and snow zone is row 3. Vertical dashed grey lines are indicative of monthly, annual and decadal timescales respectively.

3.4.4 Correlation between teleconnections and extreme weather (wtc response)

The wtc is an analysis of the coherency between the two data sets at range of scales and through time and results are shown for each weather time series on SOI or PDO in Figures 3.9, 3.10 and 3.11. For each Figure column 1 shows the PDO results where column 2 shows the SOI response. The wtc is used to identify periods within two time series which are covarying, where low power indicates low coherency and high power indicates local correlation between 2 cwt's (Grinsted et al., 2004).

Precipitation and Teleconnections

The average arid, warm temperate and snow zone $wtc(ppt, soi)$ decompositions are shown in Figure 3.9, column 1(3.9a, 3.9b and 3.9c). Figure 3.9d, 3.9e and 3.9f show the same but for $wtc(ppt, pdo)$.

For $wtc(ppt, pdo)$ the arid zone indicates that BSk and BWh have significantly different responses for extreme precipitation at 128 days and 512 days (BSk) and 256 days for BWh. The warm temperate zone shows that Cfa and Csb indicate significant differences within the periods of 32-512 days. Where the snow zone indicates later scales for significance at 128-512 for both Dfa and Dfb with an additional scale at 32 days for Dfb. High coherency is found with a peak at the annual timescale, which illustrates that the annual signal of precipitation is correlated with both teleconnections.

For the $wtc(ppt, soi)$ the arid zone contains significantly different scales within the BSk at 32-256, the BWh at 64 and the BWK region at 64 and 256 days. The warm temperate zone shows significant scales within the Cfa region at 32-1024 days, and not so many for Csa and Csb at 64 and 32-256 days, respectively. For the snow zone

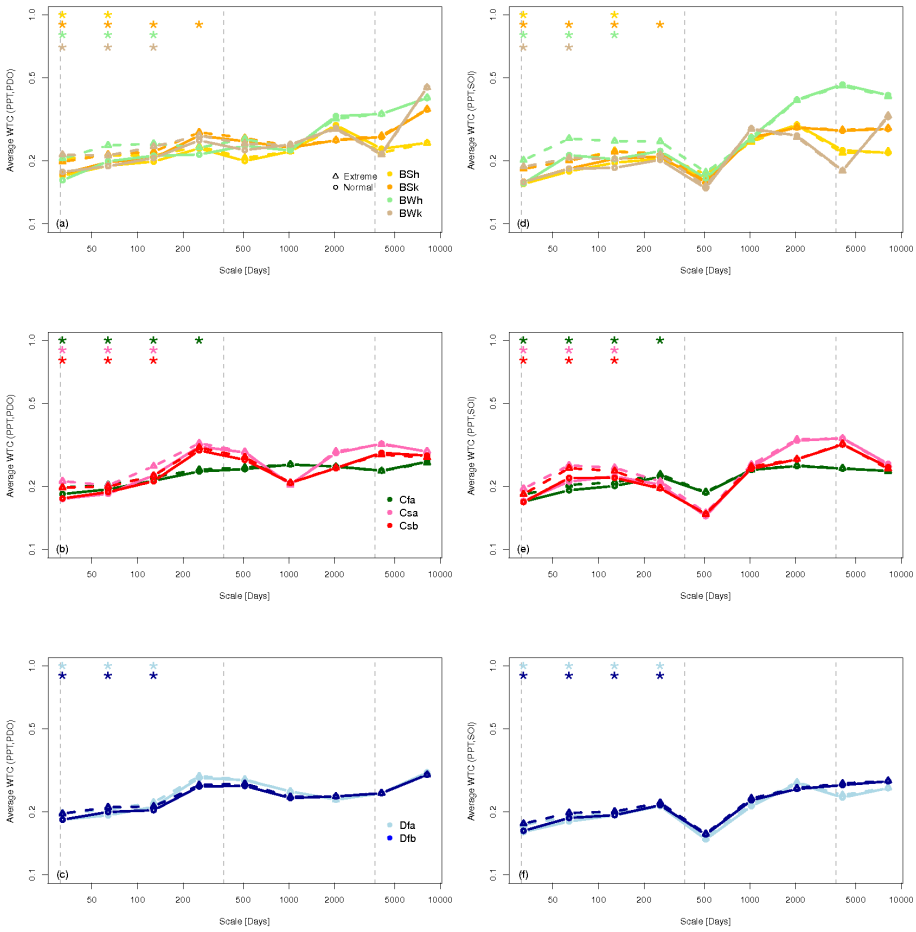

Figure 3.9 Wavelet coherence transform (*wtc*) results of precipitation and teleconnections. Extreme (dashed) and normal (solid) results averaged across each Koeppen-Geiger region, where the arid zone is row 1, warm temperate zone is row 2 and snow zone is row 3. Vertical dashed grey lines are indicative of monthly, annual and decadal timescales respectively.

the significance can be found in for Dfa and Dfb at 32-256 days or a period of 512 days, respectively. One difference is that the instead of high coherency at the annual the ppt, soi shows the opposite trend than ppt, pdo.

Maximum Temperature and Teleconnections

The average arid, warm temperate and snow zone $wtc(tmax, soi)$ decompositions are shown in Figure 3.10, column 1(3.10a, 3.10b and 3.10c). Figure 3.10d, 3.10e and 3.10f show the same but for $wtc(tmax, pdo)$.

The $wtc(tmax, pdo)$ results indicate that for the arid zone the different responses occur within BSh (32 and 64 days), BSk (between 32-256 days), BWh (32-128 days) and BWk (32 and 64 days). For the warm temperate zone, Cfa at periods of (32-256 days) and Csa/Csb at (32-128 days). Lastly the snow zone within Dfa and Dfb at 32-128.

The $wtc(tmax, soi)$ results indicate similar results. For the arid zone, BSh at 32 and 64 days, BSk between 32-256 days, BWh between 32-128 days and BWk at 32 and 64 days. Within the warm temperate zone, Cfa within periods of 32-256 days and Csa/Csb within periods of 32-128 days. Lastly the snow zone indicates significantly different trends in the coherency for maximum temperature within Dfa and Dfb at the periods of 32-256 days.

Minimum Temperature and Teleconnections

The average arid, warm temperate and snow zone $wtc(tmin, soi)$ power spectras are shown in Figure 3.11, column 1(3.11a, 3.11b and 3.11c). Figure 3.11d, 3.11e and 3.11f show the same but for $wtc(tmin, pdo)$.

The $wtc(tmin, pdo)$ results indicate the arid zones have significantly different coherency for the BSh and BSk at periods of 256 and 512 days respectively. Within

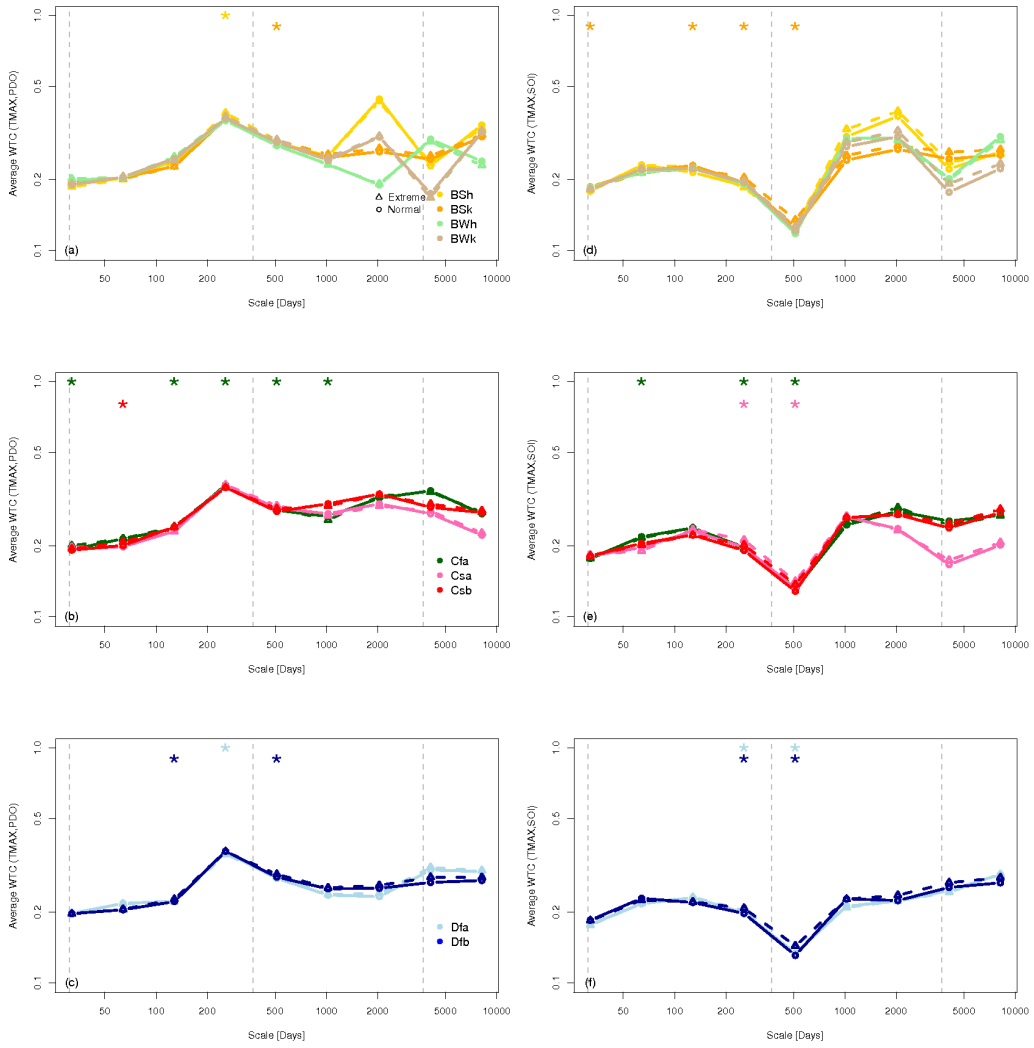

Figure 3.10 Wavelet coherence transform (*wtc*) results of maximum temperature and teleconnections. Extreme (dashed) and normal (solid) results averaged across each Koeppen-Geiger region, where the arid zone is row 1, warm temperate zone is row 2 and snow zone is row 3. Vertical dashed grey lines are indicative of monthly, annual and decadal timescales respectively.

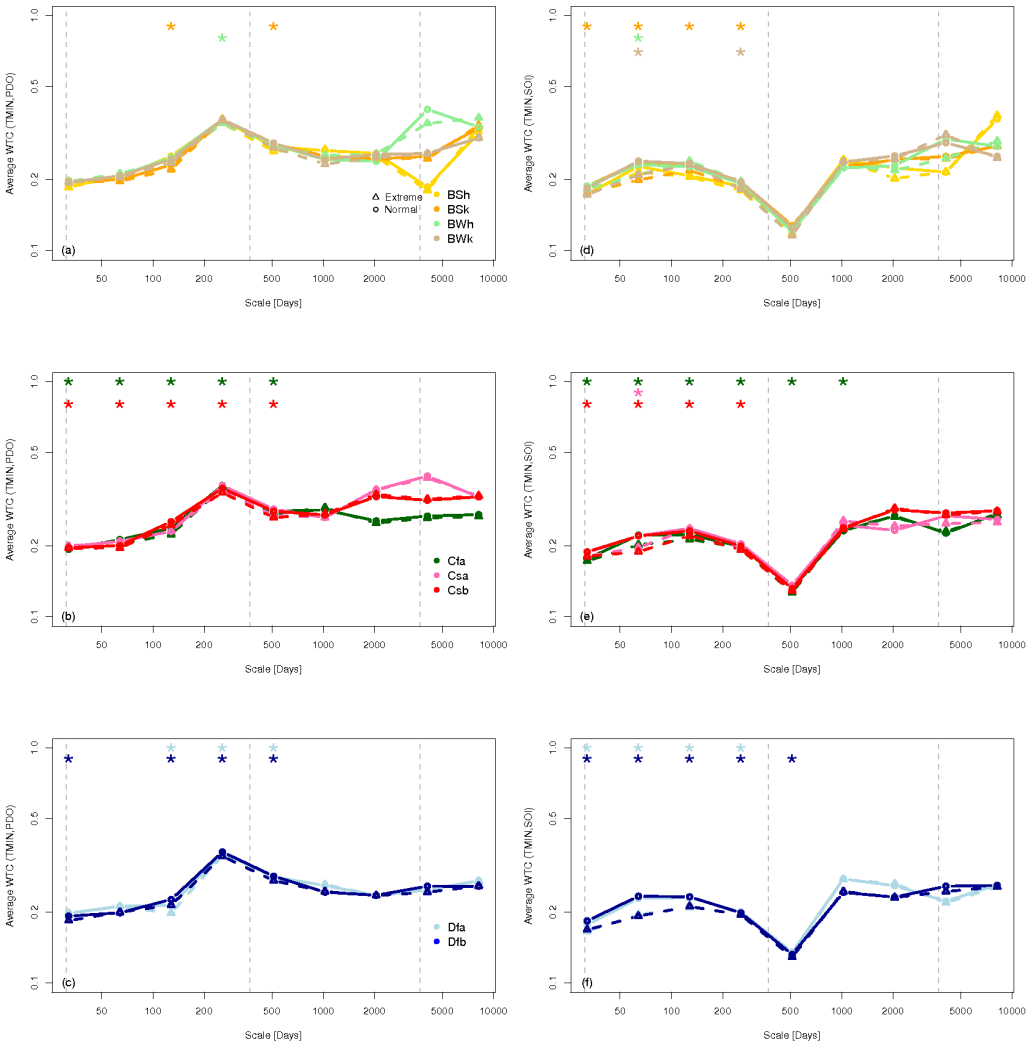

Figure 3.11 Wavelet coherence transform (*wtc*) results of minimum temperature and teleconnections. Extreme (dashed) and normal (solid) results averaged across each Koeppen-Geiger region, where the arid zone is row 1, warm temperate zone is row 2 and snow zone is row 3. Vertical dashed grey lines are indicative of monthly, annual and decadal timescales respectively.

the warm temperature zone Cfa at a period of 32 days and 128-1024 days as well as Csb at 64 days. Lastly the snow zone indicate that Dfa at 256 days and Dfb at 128 days and 1024 days have different coherency for extreme against those of a normal minimum temperature and PDO.

The $wtc(tmin, soi)$ results that for minimum temperature and SOI shows a significantly different correlation between the two time series in only one of the arid regions, BSh at 32 and within the periods of 128-512 days. For the warm temperate zone a similar result can be found in the Cfa region at 64 days, 256 days and 512 days and in the Csa region at periods of 256-512 days. Lastly the snow zone indicates that Dfa and Dfb show significantly different signals at the 256-512 days ranges.

3.5 Discussion

Wavelet analysis is been applied throughout recent literature to identify and isolate the natural climatic components in global climate change. Specifically within the hydrological cycle, Nakken (1999) used a Morlet spectrum analysis in the last century the relationship in the past 100 years between SOI on hydrologic extremes changed. Reasonable physical relationships between weather and climate forcings are also confirmed confirmed by cross-wavelet analyses (Labat, 2008). Due to its nonlinear structure, the climate system shows quite high natural variability at multiple timescales. Monsoonal relationships have also been understood using wavelets, where negative PDO period (1947-1976), indicated 7 of the 10 wet monsoon years were associated with a La Niña event or the year after (Chan, 2005). Beside a shift of the mean states and of extreme values of climate variables, climate change may also change the frequency or the spatial patterns of these natural climate variations (Janicke et al., 2009). In southwestern Canada, statistically significant interannual

and interdecadal oscillations that occurred alongside seasonal precipitation anomalies (Gan et al., 2007).

Rossi et al. (2011) found that common distributions are observed for all climate indices, which suggests teleconnection signals are somewhat connected in their evolution and total variance over time. There have been reasonable physical relationships between hydrological cycle oscillations and teleconnections and Labat (2008) investigated specifically ENSO and river runoff in North America and confirmed heavy precipitation and ENSO connectivity through cross-wavelet analyses. Using wavelets, statistically significant interannual and interdecadal oscillations can be linked with anomalies. At interannual scales, station precipitation from (Gan et al., 2007) anomalies show unstable relations with large-scale climate anomalies such as ENSO and PDO.

The most significantly different extreme weather events found are within the extreme precipitation results. In terms of the *cwt* response all three zones are indicative of a separation in power spectra up until the annual timescale, that is nation wide there is a significantly different response between extreme and normal daily rainfall. This result also is apparent in the *xwt* and *wtc* results as well. Extreme precipitation demonstrates a separation in all three climate zones as well for cross power response due to SOI forcing. In terms of coherency (*wtc*) extreme precipitation and normal precipitation seem to follow the same pattern but the result of interest here is that PDO has a peak which indicated high power and high coherency, where SOI shows the opposite behavior at the 500 day period. This is interesting and indicated that all climate zones response differently to PDO or SOI.

In regards to extreme temperature events, there is not an overwhelming conclusion from the minimum temperature events. Though within the arid zone there are significant differences in the daily maximum temperature results. This is illustrated

in the cross power results (xwt) where the SOI forcing has a distinct separation in power.

3.6 Conclusion

Overall, extreme weather events behave differently than normal events on specific timescales within different climate zones. The cwt results indicate that extreme precipitation separates from the normal at less than annual timescales. For maximum temperature, both extreme and normal events contain significant signals at the monthly timescale. For minimum temperature there are not many significant results in terms of the difference in extreme and normal responses. A significant difference is seen in the snow zone, which indicates extreme cold events vary in a different power spectra than normal.

The xwt results are indicative of phase differences and similarities between the time series and teleconnection patterns. Precipitation and SOI interactions are mostly significant at all scales while precipitation and PDO are only significantly different below the annual timescale. As both teleconnection patterns and precipitation spectra results move through time they become more in phase with each other, which indicates the precipitation has a high power spectrum which is significant on longer timescales, indicative of ENSO and PDO. In terms of xwt, results for temperature both maximum and minimum temperate exhibit similar results. Both peaking in phase consistency around the annual timescale, indicating that the annual temperature cycle is a dominate feature. In terms of separating normal from extreme events, this occurs in the longer timescales, and only within a few regions, indicating the sensitive nature of ENSO and PDO on temperature events.

The wtc results show how correlated two decompositions are, in this case extreme

weather and either SOI or PDO. For all three extreme weather events there is an opposing peak of high correlation at the annual timescale for all the PDO transforms and a peak of low correlation between all the SOI transforms. The warm temperate zone shows many significantly different scales for precipitation while for temperature the majority of the differences can be found in the snow zone. This indicates there is more variability in warm temperature extreme precipitation and the role teleconnections play while the snow zone is most sensitive to temperature and teleconnection interactions.

Understanding the influence of regional teleconnections may enhances the ability to forecast extreme weather. Results from this paper suggest extreme precipitation is more sensitive to teleconnection patterns over the entire US and that the snow zones are showing a distinct separation in scale dynamics for temperature events. With a better understanding of the natural variability in the climate system, better projections can be made for the future.

Chapter 4

Conclusion

This thesis has addressed how extreme weather events have changed in the past 100 years and how they are correlated with teleconnection patterns. Changes in extreme precipitation events are an order of magnitude smaller than the number of extreme temperature events. The northeast half of the country have exhibited the greatest extremes in precipitation. Extreme maximum temperate events are decreasing by about 20 events (per 100 years) in the last century within the Eastern US, and increasing by around 20 events (per 100 years) over the Western states. The trend in a reduction of extreme temperature is present across all seasons and throughout all climate zones, with exception of the Southeast. With the projected increase of overall global temperature these extremes will only continue to vary.

Overall, extreme weather events behave differently than normal events on specific timescales within different climate zones. Although the trends in extreme precipitation are an order of magnitude smaller than temperature, the behavior of those events varies significantly from normal events. Extreme precipitation is largely influenced by teleconnections. As more variability is introduced into the climate, regional circulation patterns may be altered and in turn have a larger impact on extremes.

The findings of this thesis can provide a pathway to future research topics in areas such as agronomy, ecology, geography and public policy. Future research topics could include understanding the growing season dynamics and the influence of extreme events on agriculture, what plant species and animal species are impacted by extreme events, and how are their climates are changing. There are many geographical outlets for this research, like visualization, human impacts and further linkages to physical forcing mechanism such as soil structure and other aspects of regional climate. Lastly, this information can be used to assist policy makers in assessment of past environmental decisions and most importantly, future changes.

Climate change has no boundaries; it will affect everyone from agricultural societies to urban dwellers. Heat and cold waves, floods and drought, all have the potential to greatly impact facets of our daily lives, from, crop yields to water supply to health and industry. The ramifications of climate change are already being seen across the country, growing seasons are showing earlier onset, the fight for water is already prevalent and industries are struggling to adapt.

Bibliography

Alexander, L. V., et al., 2006: Global observed changes in daily climate extremes of temperature and precipitation. *Journal of Geophysical Research*, **111 (D5)**.

Allan, R. P. and B. J. Soden, 2008: Atmospheric Warming and the Amplification of Precipitation Extremes. *Science*, **321 (5895)**, 1481–1484.

Anderson, A. and A. Kostinski, 2011: Evolution and Distribution of Record-Breaking High and Low Monthly Mean Temperatures. *Journal of Applied Meteorology and Climatology*, **50 (9)**, 1859–1871.

Anderson, B. T., 2011: Near-term increase in frequency of seasonal temperature extremes prior to the 2 °C global warming target. *Climatic Change*, **108 (3)**, 581–589.

Barlow, M., S. Nigam, and E. H. Berbery, 2001: ENSO, Pacific decadal variability, and US summertime precipitation, drought, and stream flow. *Journal of Climate*, **14 (9)**, 2105–2128.

Battisti, D. S. and R. L. Naylor, 2009: Historical Warnings of Future Food Insecurity with Unprecedented Seasonal Heat. *Science*, **323 (5911)**, 240–244.

Blekinsop, S., P. Jones, S. Dorling, and T. Osborn, 2008: Observed and modelled

influence of atmospheric circulation on central England temperature extremes. *International Journal of Climatology*, **29 (11)**, 1642–1660.

Booth, E. L. J., J. M. Byrne, and D. L. Johnson, 2011: Climatic changes in western North America, 1950-2005. *International Journal of Climatology*.

Cayan, D. R., K. T. Redmond, and L. G. Riddle, 1999: ENSO and Hydrologic Extremes in the Western United States*. *Journal of Climate*, **12 (9)**, 2881–2893.

Chan, J. C. L., 2005: PDO, ENSO and the early summer monsoon rainfall over south China. *Geophysical Research Letters*, **32 (8)**, L08 810.

Chou, C., C.-A. Chen, P.-H. Tan, and K. T. Chen, 2012: Mechanisms for Global Warming Impacts on Precipitation Frequency and Intensity. *Journal of Climate*, **25 (9)**, 3291–3306.

Clark, R. T., J. M. Murphy, and S. J. Brown, 2010: Do global warming targets limit heatwave risk? *Geophysical Research Letters*, **37 (17)**, L17 703–.

Diez, J. M., et al., 2012: Will extreme climatic events facilitate biological invasions? *Frontiers in Ecology and the Environment*, **10 (5)**, 249–257.

Easterling, D. R., J. Evans, P. Groisman, T. Karl, K. Kunkel, and P. Ambenje, 2000: Observed variability and trends in extreme climate events: a brief review. *Bulletin of the American Meteorological Society*, **81 (3)**, 417–426.

Gan, T. Y., A. K. Gobena, and Q. Wang, 2007: Precipitation of southwestern Canada: Wavelet, scaling, multifractal analysis, and teleconnection to climate anomalies. *Journal of Geophysical Research: Atmospheres (1984–2012)*, **112 (D10)**.

Gershunov, A. and T. P. Barnett, 1998: Interdecadal modulation of ENSO teleconnections. *Bulletin of the American Meteorological Society*, **79**, 2715–2726.

Gouhier, T. and A. Grinsted, 2013: Biwavelet (R package).

Grinsted, A., J. C. Moore, and S. Jevrejeva, 2004: Application of the cross wavelet transform and wavelet coherence to geophysical time series. *Nonlinear Processes in Geophysics*, **11 (5/6)**, 561–566.

Groisman, P. Y., R. W. Knight, and T. R. Karl, 2001: Heavy precipitation and high streamflow in the contiguous United states : Trends in the twentieth century. *Bulletin of the American Meteorological Society*, **82 (2)**, 219–246.

Groisman, P. Y., R. W. Knight, and T. R. Karl, 2012: Changes in Intense Precipitation over the Central United States. *Journal of Hydrometeorology*, **13 (1)**, 47–66.

Gutowski, W. J., Jr., et al., 2010: Regional Extreme Monthly Precipitation Simulated by NARCCAP RCMs. *Journal of Hydrometeorology*, **11 (6)**, 1373–1379.

Hayhoe, K., et al., 2006: Past and future changes in climate and hydrological indicators in the US Northeast. *Climate Dynamics*, **28 (4)**, 381–407.

Held, I., 2000: Water Vapor Feedback and Global Warming 1. *Annual Review of Energy and the Environment*, **25**, 441–475.

Higgins, R. W., A. Leetmaa, Y. Xue, and A. Barnston, 2000: Dominant factors influencing the seasonal predictability of US precipitation and surface air temperature. *Journal of Climate*, **13 (22)**, 3994–4017.

Hughes, P., 1982: Weather, Climate, and the Economy. *Weatherwise*, **35 (2)**, 60–63.

IPCC, 2001: Climate Change 2001: Impacts, Adaptation and Vulnerability. IPCC Third Assessment Report. Cambridge Univeristy Press, Cambridge, UK.

IPCC, 2007: Climate Change 2007: The physical science basis: contribution of Working Group I to the Fourth Assessment Report of the Intergovernmental Panel on Cliamte Change. Cambridge Univeristy Press, Cambridge, UK.

IPCCSREX, 2012: Managing the Risks of Extreme Events and Disasters to Advance Climate Change Adaptation. *Cambridge Univeristy Press*, 1–594.

Janicke, H., M. Bottinger, U. Mikolajewicz, and G. Scheuermann, 2009: Visual Exploration of Climate Variability Changes Using Wavelet Analysis. *IEEE Transactions on Visualization and Computer Graphics*, **15 (6)**, 1375–1382.

Karl, T., et al., 1995: Critical issues for long-term climate monitoring. *Climatic Change*, **31 (2)**, 185–221.

Kleeman, R., 2002: Measuring dynamical prediction utility using relative entropy. *Journal of the atmospheric sciences*, 1–16.

Knight, R., 1998: Secular trends of precipitation amount, frequency, and intensity in the United States. *Bulletin of the American Meteorological Society*, **79 (2)**, 231–241.

Knutson, T. R. and S. Manabe, 1995: Time-Mean Response over the Tropical Pacific to Increased C0 2in a Coupled Ocean-Atmosphere Model. *Journal of Climate*, **8 (9)**, 2181–2199.

Knutti, R., et al., 2008: A Review of Uncertainties in Global Temperature Projections over the Twenty-First Century. *Journal of Climate*, **21 (11)**, 2651–2663.

Kottek, M., J. Grieser, C. Beck, B. Rudolf, and F. Rubel, 2006: World Map of the Köppen-Geiger climate classification updated. *Meteorologische Zeitschrift*, **15 (3)**, 259–263.

Kunkel, K. E., K. Andsager, and D. R. Easterling, 1999: Long-Term Trends in Extreme Precipitation Events over the Conterminous United States and Canada. *Journal of Climate*, **12**, 2515–2527.

Kunkel, K. E., D. R. Easterling, K. Redmond, and K. Hubbard, 2003: Temporal variations of extreme precipitation events in the United States: 1895-2000. *Geophysical Research Letters*, **30 (17)**, 1900–1905.

Labat, D., 2008: Wavelet analysis of the annual discharge records of the world's largest rivers. *Advances in water resources*, **31 (1)**, 109–117.

Latif, M., A. Timmermann, J. Oberhuber, A. Bacher, M. Esch, and E. Roeckner, 1999: Increased El Nino frequency in a climate model forced by future greenhouse warming : Abstract : Nature. *Nature*, **398 (6729)**, 694–697.

Lenderink, G. and E. van Meijgaard, 2008: Increase in hourly precipitation extremes beyond expectations from temperature changes. *Nature Geoscience*, **1 (8)**, 511–514.

Mantua, N., S. Hare, Y. Zhang, J. Wallace, and R. Francis, 1997: AMS Journals Online - A Pacific Interdecadal Climate Oscillation with Impacts on Salmon Production. *Bulletin of the American Meteorological Society*, **78**, 1069–1079.

McCabe, G. J. and M. D. Dettinger, 1999: Decadal variations in the strength of ENSO teleconnections with precipitation in the western United States. *International Journal of Climatology*, **19 (13)**, 1399–1410.

Meehl, G. and W. M. Washington, 1996: El Niño-like climate change in a model with increased atmospheric CO 2 concentrations. *Nature*, **382**, 56–60.

Meehl, G. A., J. M. Arblaster, and C. Tebaldi, 2007a: Contributions of natural and

anthropogenic forcing to changes in temperature extremes over the United States. *Geophysical Research Letters*, **34 (19)**.

Meehl, G. A., A. Hu, and C. Tebaldi, 2010: Decadal Prediction in the Pacific Region. *Journal of Climate*, **23 (11)**, 2959–2973.

Meehl, G. A., C. Tebaldi, H. Teng, and T. C. Peterson, 2007b: Current and future U.S. weather extremes and El Niño. *Geophysical Research Letters*, **34 (20)**, L20 704.

Meehl, G. A., C. Tebaldi, G. Walton, D. Easterling, and L. McDaniel, 2009: Relative increase of record high maximum temperatures compared to record low minimum temperatures in the U.S. *Geophysical Research Letters*, **36 (23)**, L23 700–L23 705.

Menne, M., C. Williams, Jr, and R. Vose, 2011: United States Historical Climatology Network Daily Temperature, Precipiation, and Snow Data. Carbon Dioxide Information Analysis Center, Oak Ridge National Laboratory.

Nakken, M., 1999: Wavelet analysis of rainfall–runoff variability isolating climatic from anthropogenic patterns. *Environmental Modelling & Software*, **14 (4)**, 283–295.

Neelin, J. D., D. S. Battisti, A. C. Hirst, F.-F. Jin, Y. Wakata, T. Yamagata, and S. E. Zebiak, 1998: ENSO theory. *Journal of Geophysical Research*, **103 (C7)**, 14 261–14 290.

Nigam, S., M. Barlow, and E. Berbery, 1999: Analysis Links Pacific Decadal Variability to Drought and Streamflow in United States. *EOS*, **80**, 1–8.

Onoz, B. and M. Bayazit, 2003: The power of statistical tests for trend detection. *Turkish Journal of Engineering and Environmental Sciences*, **27 (4)**, 247–251.

Pielke, R. A., Jr and M. W. Downton, 2000: Precipitation and Damaging Floods: Trends in the United States, 1932–97. *Journal of Climate*, **13**, 36253 637.

Portmann, R., S. Solomon, and G. Hegerl, 2009: Spatial and seasonal patterns in climate change, temperatures, and precipitation across the United States. *Proceedings of the National Academy of Sciences*, 1–6.

Riebsame, W. E., S. A. J. Changnon, and T. Karl, 1991: *Drought and natural resources management in the United States. Impacts and implications of the 1987-89 drought.* Westview Press Inc.

Ropelewski, C. F. and M. S. Halpert, 1986: North American precipitation and temperature patterns associated with the El Niño/Southern Oscillation (ENSO). *Monthly Weather Review*, **114 (12)**, 2352–2362.

Rossi, A., N. Massei, and B. Laignel, 2011: A synthesis of the time-scale variability of commonly used climate indices using continuous wavelet transform. *Global and Planetary Change*, **78 (1-2)**, 1–13.

Santer, B., et al., 2007: Identification of human-induced changes in atmospheric moisture content. *Proceedings of the National Academy of Sciences*, **104 (39)**, 15 248–15 253.

Smith, T. M. and C. F. Ropelewski, 1997: Quantifying Southern Oscillation-precipitation relationships from an atmospheric GCM. *Journal of Climate*, **10 (9)**, 2277–2284.

Stenseth, N. C., 2002: Ecological Effects of Climate Fluctuations. *Science*, **297 (5585)**, 1292–1296.

Tebaldi, C., K. Hayhoe, J. M. Arblaster, and G. A. Meehl, 2006: Going to the Extremes. *Climatic Change*, **79 (3-4)**, 185–211.

Torrence, C., 1998: A practical guide to wavelet analysis. *Bulletin of the American Meteorological Society*, **79 (1)**, 61–78.

Torrence, C. and P. J. Webster, 1998: The annual cycle of persistence in the El Nño/Southern Oscillation. *Quarterly Journal of the Royal Meteorological Society*, **124 (550)**, 1985–2004.

Trenberth, K. and A. Dai, 2003: The changing character of precipitation. *Bulletin of the American Meteorological Society*, 1205–1217.

Trenberth, K. E., 1984: Signal versus noise in the Southern Oscillation. *Monthly Weather Review*, **112**, 326–332.

Trenberth, K. E., 2009: *Climate system modeling, Cambridge University Press (Cambridge)*, Vol. 1. Cambridge University Press.

Weng, H., K. Lau, and Y. Xue, 1999: Multi-scale summer rainfall variability over China and its long-term link to global sea surface temperature variability. *Journal of the Meteorological Society of Japan*, **77 (4)**, 845–857.

Wilson, C. J., N. A. Brunsell, C. B. Young, L. M. Miller, and D. B. Mechem, 2013: Trends in 20th Century Weather Extremes over the Contiguous United States. *Journal of Applied Meteorology and Climatology*, (in review).

Wolter, K., R. M. Dole, and C. A. Smith, 1999: Short-term climate extremes over the continental United States and ENSO. Part I: Seasonal temperatures. *Journal of Climate*, **12 (11)**, 3255–3272.

Zhang, Y., J. M. Wallace, and D. S. Battisti, 1997: ENSO-like Interdecadal Variability: 1900–93. *Journal of Climate*, **10 (5)**, 1004–1020.

Zwiers, F. W., X. Zhang, and Y. Feng, 2011: Anthropogenic Influence on Long Return Period Daily Temperature Extremes at Regional Scales. *Journal of Climate*, **24 (3)**, 881–892.